Asymmetric Cooper pair transistor in parallel to a dc SQUID: Two coupled quantum systems

A. Fay,[1,*] W. Guichard,[1] O. Buisson,[1] and F. W. J. Hekking[2]
[1]*Institut Néel, CNRS–Université Joseph Fourier, BP 166, F-38042 Grenoble Cedex 9, France*
[2]*LPMMC, CNRS–Université Joseph Fourier, BP 166, F-38042 Grenoble Cedex 9, France*
(Received 26 November 2010; revised manuscript received 25 February 2011; published 17 May 2011)

We present a theoretical analysis of a superconducting quantum circuit based on a highly asymmetric Cooper pair transistor (ACPT) in parallel to a dc superconduction quantum intereference device (SQUID). Starting from the full Hamiltonian we show that the circuit can be modeled as a charge qubit (ACPT) coupled to an anharmonic oscillator (dc SQUID). Depending on the anharmonicity of the SQUID, the Hamiltonian can be reduced either to one that describes two coupled qubits or to the Jaynes-Cummings Hamiltonian. Here the dc SQUID can be viewed as a tunable micrometer-sized resonator. The coupling term, which is a combination of a capacitive and a Josephson coupling between the two qubits, can be tuned from the very strong- to the zero-coupling regime. It describes very precisely the tunable coupling strength measured in this circuit [A. Fay *et al.*, Phys. Rev. Lett. **100**, 187003 (2008)] and explains the "quantronium" as well as the adiabatic quantum transfer readout.

DOI: 10.1103/PhysRevB.83.184510 PACS number(s): 85.25.Cp, 03.67.Lx, 74.50.+r

I. INTRODUCTION

Two quantum systems with discrete energy levels coupled to each other form an elementary block, useful for the study of fundamental phenomena and effects in quantum physics, especially in the context of quantum information. The interaction between the two quantum systems is essential to implement important concepts in this field such as entanglement, quantum gate operations, and quantum information transfer. As to the theoretical description of interacting quantum systems, two problems have been extensively studied in particular: a two-level system (or qubit) coupled to a harmonic oscillator and two coupled qubits. The former was used to describe among others the quantum electrodynamics associated with atoms in a cavity,[1] trapped ions coupled to their vibrations,[2] and, more generally, interaction between matter and photons.[3] The latter was developed to describe entangled photons, trapped ions, and two-qubit quantum gate operations.[4]

These studies were experimentally realized in the fields of quantum optics and atomic physics and more recently extended to include quantum solid-state devices. In particular, during the past decade superconducting circuits have demonstrated their potential in connection with quantum experiments.[5–14] They now appear as experimental model systems for studying fundamental quantum physics and basic blocks for quantum information.

In this paper we consider a superconducting circuit composed of two well-known elements coupled to each other: an inductive dc superconducting quantum interference device (SQUID) and a Cooper pair transistor. This circuit constitutes an elementary building block that can be operated in various parameter regimes characterized by different types of quantum dynamics, as has been shown experimentally in the past. As we will detail below, this is possibly due to the fact that three strongly coupled quantum variables determine the dynamics of this coupled circuit.

For instance, when the current-biased dc SQUID is noninductive and classical and the transistor is symmetric, one recovers the quantronium.[15] When the SQUID is operated in the nonlinear regime, the resulting system consists of a charge qubit coupled to an anharmonic oscillator; this system has been shown to allow for nondestructive quantum measurements.[16] We recently operated the SQUID in the quantum few-level limit,[17] demonstrating a very strong tunable coupling between two different types of qubit: a phase qubit and a charge qubit.

The experimental performance of this circuit was limited by uncontrolled decoherence sources. However, its integration (three quantum variables strongly coupled on a micrometer scale), its tunability, and its various optimal points make this circuit attractive once decoherence sources will be overcome upon technological improvements.

In this paper we present a rigorous theoretical analysis of the circuit in the parameter range of our experiments.[17] The full Hamiltonian of the coupled circuit is presented, describing a two-level system (Cooper pair transistor) coupled to two anharmonic oscillators (dc SQUID). In the relevant parameter range, the dc SQUID dynamics can be reduced from two dimensional to one dimensional. Consequently the dynamics of the circuit is that of a qubit coupled to a single anharmonic oscillator. Depending on the anharmonicity, different regimes can be studied in this unique circuit. When the anharmonicity is neglected, we recover the physics of a qubit coupled to a harmonic oscillator. The quantum properties of this circuit are then described by the well-known Jaynes-Cummings Hamiltonian. Although this limit can also be achieved with a qubit coupled to a high-Q coplanar waveguide cavity,[5,18] we wish to emphasize that the use of a dc SQUID is of interest as it constitutes a micrometer-sized resonator and it is tunable. When the oscillator is considered anharmonic, its interaction with a qubit gives rise to very complex dynamics, which has not been explored thoroughly. If only the two lowest levels of the oscillator are considered, it can be reduced to a two-level system. The coupled circuit then describes two interacting qubits. In addition to the possibility to study different dynamical regimes depending on the anharmonicity of the resonator, the coupling between the SQUID and the

transistor is fully tunable. As a result, the system can be operated at zero coupling, as well as in the weak and in the strong coupling limits.

In Sec. II, after a description of the circuit under consideration, we construct the Lagrangian and the Hamiltonian following Yurke *et al.*[19] and Devoret.[20] Section III is devoted to the two-dimensional Hamiltonian of an inductive SQUID and its reduction to one-dimensional Hamiltonian in the relevant parameter range. In Sec. IV we discuss the Hamiltonian of the asymmetric Cooper pair transistor (ACPT), especially at its two optimal points where it is insensitive to noise fluctuations. In Sec. V the terms describing the coupling between the dc SQUID and the transistor are discussed. In Sec. VI, the full Hamiltonian of the coupled circuit is rewritten in the eigenbasis of the dc SQUID and the ACPT for the two different anhamonicity regimes of the dc SQUID. There we also discuss the two possible quantum measurements of the charge qubit that can be performed by the dc SQUID. The last section discusses the tunable coupling strength of the circuit and its comparison with the experiments.

II. COUPLED CIRCUIT HAMILTONIAN

A general theory for analyzing the quantum behavior of complex electronic circuits was originally established by Yurke *et al.*[19] and extended to study nonlinear superconducting circuits containing qubits.[20,21] However, to the best of our knowledge, only the persistent current qubit has been treated in a theoretical article using a rigorous circuit theory by Orlando *et al.*[22] In most situations, in order to analyze experimental results obtained for a given circuit, an intuitively acceptable, effective few-level Hamiltonian valid at low energies is postulated. The interest of presenting a rigorous analysis for the coupled circuit is to explore in detail the various regimes of the circuit. For each studied regime, the number of variables involved in the circuit dynamics is reduced by using assumptions which are well defined and conditions that can be clearly stated.

A. Circuit description

A schematic electronic representation of the circuit studied theoretically hereafter is presented in Fig. 1(b). In this circuit two different elements are coupled that correspond to two basic blocks for typical superconducting quantum devices. The first element is a dc SQUID; it corresponds to a loop which contains two identical Josephson junctions (JJs), each with a critical current I_0 and a capacitance C_0. The total inductance L_S of the dc SQUID is the sum of three inductances L_1, L_2, and L_3, associated with the different parts of the SQUID loop. The second element of the circuit is an ACPT which is placed in parallel with the dc SQUID. The ACPT consists of a superconducting island connected to the dc SQUID by two different JJs. We denote by I_1^T and I_2^T the critical currents and C_1^T and C_2^T the capacitances of these junctions. The asymmetry of the transistor is characterized by the Josephson asymmetry parameter $\mu = (I_2^T - I_1^T)/(I_2^T + I_1^T)$ and the capacitance asymmetry parameter $\lambda = (C_2^T - C_1^T)/(C_2^T + C_1^T)$. The ACPT is also coupled to a gate voltage; this is modeled theoretically by an infinite capacitance C_P with a charge Q_b with $C_P, Q_b \to \infty$ so the ratio $Q_b/C_b \equiv V_g$. The circuit is

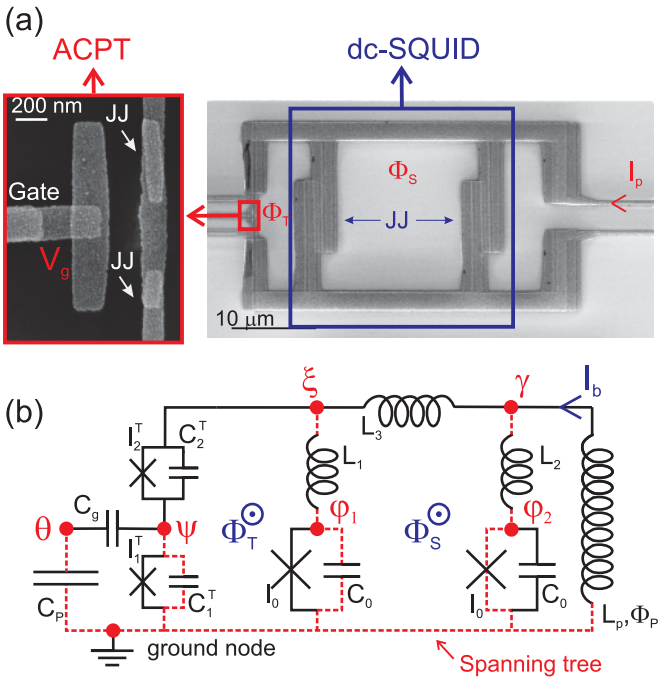

FIG. 1. (Color online) The coupled circuit studied experimentally in Ref. 17. (a) On the right-hand side, a SEM picture shows the two elements of the circuit, i.e., an ACPT (red frame) connected in parallel to a dc SQUID (blue frame). A zoom-in of the transistor is shown on the left-hand side of the SEM picture. The transistor asymmetry stems from the difference between the areas of the two JJs. The properties of the circuit can be modified by the bias current I_b, the flux Φ_S in the dc SQUID, the flux Φ_T in the other loop, and the gate voltage V_g. (b) Schematic representation of the circuit. The four JJs are represented by a pure Josephson element in parallel with a capacitance. The voltage bias of the transistor gate and the current bias of the circuit are schematically indicated by an infinite capacitance C_P and an infinite inductance L_P, respectively. The spanning tree drawn in dashed line connects the ground node to the six active nodes $\varphi_1, \varphi_2, \psi, \theta, \gamma$, and ξ.

current biased, modeled similarly with the help of an infinite inductance $L_b \to \infty$ threaded by a flux $\Phi_b \to \infty$ so that the ratio $\Phi_b/L_b \equiv I_b$ remains constant. The properties of the circuit depend on four experimentally tunable parameters V_g, I_b and the fluxes Φ_S and Φ_T threading the dc SQUID loop and the other loop of the circuit, respectively. As we will see, these parameters allow to control and change the physics of the coupled circuit. This circuit, realized and studied experimentally by Fay *et al.*,[17] is shown in the scanning electron microscope (SEM) view in Fig. 1(a).

B. Quantum circuit theory

The relevant degrees of freedom of a superconducting circuit and their dynamics can be determined using the concept of node phases introduced by Devoret.[20] We distinguish two different kinds of nodes in the circuit. We first choose a ground node to which the zero of phase is associated. Note that this choice corresponds to a choice of gauge and is therefore arbitrary, although this choice affects the detailed form of the Hamiltonian it does not affect the resulting dynamics of the circuit. The other nodes of the circuit are called the active

nodes, each described by an active phase. Six active phases are present in the circuit considered here; they are denoted by φ_1, φ_2, ψ, θ, γ, and ξ.

Let us now introduce the so-called spanning tree.[20] Starting from the ground node we draw the branches of the spanning tree, reaching each active node via a unique path. In the case of the coupled circuit, the spanning tree [drawn in dashed line in Fig. 1(b)], connects the ground node (bottom node) to the six active nodes.

The superconducting phase difference across a dipole in a superconducting circuit can be written as a function of the node phases with the help of two rules. We will illustrate these rules with the help of the circuit presented in Fig. 2 as an example. Here, three dipoles are placed in a loop threaded by the flux Φ. In this case, there are three nodes; the spanning tree (drawn in dashed line) connects the ground node to the two active nodes with phases ϕ_A and ϕ_B, respectively. As a first rule, the superconducting phase difference across a dipole located on the spanning tree is given by the difference of the phases of the nodes linked to the dipole. Hence, the superconducting phases Λ_1 and Λ_3 of the dipoles 1 and 3, respectively, are given by $\Lambda_1 = \phi_A$ and $\Lambda_2 = \phi_B$. As a second rule, in the case of a dipole which is not located on the spanning tree, we first define a minimal loop which contains the previous dipole and the other dipoles located on the spanning tree. The superconducting phase difference across the dipole is calculated, using the quantization of the phase for the minimal loop.[23] Let us apply this rule to determine the superconducting phase difference Λ_2 across dipole 2. The minimal loop corresponds simply to the loop of the circuit. The phase quantization in this loop gives $\Lambda_2 = \phi_B - \phi_A - 2\pi\Phi/\Phi_0$, with Φ_0 the superconducting flux quantum. With the help of the two previous rules, we have analyzed the coupled circuit and expressed the superconducting phase difference across each dipole as a function of the six active phases.

C. Current-conservation laws

In a superconducting circuit, we find generally three different dipoles: a capacitance C, an inductance L, and a Josephson element J. The current through each of these dipoles can be expressed as a function of the superconducting

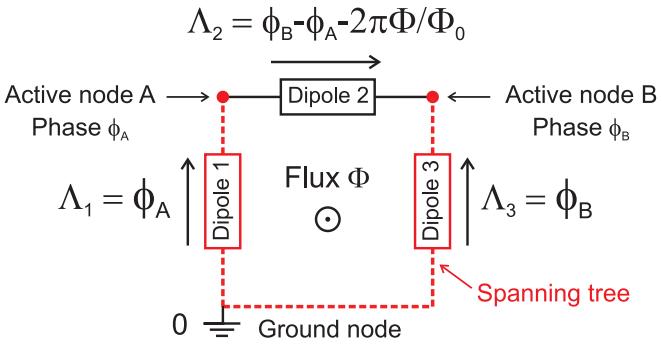

FIG. 2. (Color online) Three dipoles in a loop threaded by the flux Φ. The spanning tree in dashed line connects the ground node to the two active nodes ϕ_A and ϕ_B. The superconducting phases Λ_1, Λ_2, and Λ_3 across the three dipoles, respectively, are functions of ϕ_A, ϕ_B, and Φ.

phase difference Λ across the dipole. The voltage V is related to the phase difference Λ by $V = \phi_0\dot{\Lambda}$. The current I_C through the capacitance is then given by $I_C = \phi_0 C\ddot{\Lambda}$, where $\phi_0 = \Phi_0/(2\pi)$. The current I_L through the inductance reads $I_L = \phi_0\Lambda/L$. Finally, the current through the Josephson element is given by the Josephson relation $I_J = I_0\sin(\Lambda)$, where I_0 is the Josephson critical current.[24] Using these expressions for the current, we can write the six current conservation laws for each active node in the studied circuit (the sum of the currents flowing into each node is zero). The six conservation laws yield six equations for the dynamics of the node phases (cf. Appendix A), whose solution yields the dynamics of the entire circuit.

D. The Lagrangian

The Lagrangian $\mathcal{L}$ of the circuit depends on the six node phases and their time derivatives. Let us define the vector $\vec{x} = (\varphi_1,\varphi_2,\psi,\theta,\gamma,\xi)$ formed by the six node phases of the circuit. The six Euler-Lagrange equations are defined by[25]

$$\frac{d}{dt}\left(\frac{\partial\mathcal{L}}{\partial\dot{\vec{x}}}\right) - \frac{\partial\mathcal{L}}{\partial\vec{x}} = 0. \tag{1}$$

The Lagrangian of the circuit has to be constructed in such a way that the Euler-Lagrange equations are equivalent to the current conservation equations (Appendix A). We take the Lagrangian to be of the following form:

$$\mathcal{L}(\dot{\vec{x}},\vec{x}) = T(\dot{\vec{x}}) - V(\vec{x}), \tag{2}$$

with the kinetic energy

$$T(\dot{\vec{x}}) = \phi_0^2\{\tfrac{1}{2}C_0\dot{\varphi}_1^2 + \tfrac{1}{2}C_0\dot{\varphi}_2^2 + \tfrac{1}{2}C_2^T(\dot{\xi}-\dot{\psi})^2 + \tfrac{1}{2}C_1^T\dot{\psi}^2 + \tfrac{1}{2}C_g(\dot{\psi}-\dot{\theta})^2 + \tfrac{1}{2}C_P\dot{\theta}^2\} \tag{3}$$

and the potential energy

$$V(\vec{x}) = -\phi_0\{I_0\cos(\varphi_1) + I_0\cos(\varphi_2) + I_2^T\cos(\xi-\psi-\phi_T) + I_1^T\cos(\psi)\} + \phi_0^2\left\{\frac{1}{2}\frac{(\xi-\varphi_1)^2}{L_1} + \frac{1}{2}\frac{(\gamma-\varphi_2)^2}{L_2} + \frac{1}{2}\frac{(\gamma-\xi-\phi_S)^2}{L_3} - \frac{1}{\phi_0}I_p\gamma\right\}. \tag{4}$$

The kinetic energy corresponds to the energy stored in the capacitances of the circuit, whereas the potential energy is composed of the Josephson energies (cosine terms) and the energy stored in the inductances of the circuit. From now on, we assume the SQUID inductances $L_1 = L_2$ and introduce the inductance asymmetry η defined by $L_3 = \eta L_S$.[26] Although the Lagrangian depends on six variables, the effective low-energy behavior of the circuit is determined by three variables only, as we will see below.

Let us first consider the phase variable γ. Its dynamics is that of a harmonic oscillator of frequency $\omega_\gamma = 1/\sqrt{\tilde{L}_S C_\gamma}$. Here C_γ is the capacitance of the γ node and $\tilde{L}_S = \eta(1-\eta)L_S/(1+\eta)$. Using the circuit parameters of Ref. 17 (see Appendix B), where C_γ is estimated to be smaller than 0.1 fF, the frequency ω_γ is estimated to be larger than

1 THz, i.e., larger than all the other frequencies of the circuit. Next, consider the phase variable ξ. Again using the circuit parameters of Ref. 17, we find that the characteristic inductive currents $\phi_0/L_{1,2}$ are on the order of 1 μA, much larger than the Josephson critical current I_2^T of $\sim$1 nA. In other words, the SQUID inductance is much smaller than the Josephson inductance $\sim 1/I_2^T$. Therefore, in a first approximation, the dynamics of ξ is also of the harmonic oscillator type with a frequency $\omega_\xi = \sqrt{1/\tilde{L}_S C_2^T}$. We estimate ω_ξ to be $\sim$640 GHz. This frequency is much smaller than ω_γ, but still quite high compared to the frequencies characterizing the dynamics of the variables φ_1, φ_2, ψ, and θ ($\sim$10 GHz, see below). This implies that we can use the adiabatic approximation to eliminate the fast variables γ and ξ and obtain an effective Lagrangian for the slow variables ϕ_1,ϕ_2,ξ, and θ.

In order to implement the adiabatic approximation, we write $\gamma = \gamma_0 + \delta\gamma$ and similarly $\xi = \xi_0 + \delta\xi$. Here γ_0 and ξ_0 correspond the minima of the harmonic potentials confining the motion of these variables,

$$\gamma_0(x,y) = x + \eta y + \frac{\phi_S}{2}(1-\eta) + \frac{1}{4\phi_0} L_S I_p (1-\eta^2), \quad (5)$$

$$\xi_0(x,y) = x - \eta y - \frac{\phi_S}{2}(1-\eta) + \frac{1}{4\phi_0} L_S I_p (1-\eta)^2, \quad (6)$$

where $x = (\varphi_1 + \varphi_2)/2$ and $y = (\varphi_2 - \varphi_1)/2$. Note that γ_0 and ξ_0 depend on x and y, hence they acquire slow dynamics through the phases φ_1 and φ_2. The dynamics of the deviations $\delta\gamma$ and $\delta\xi$ is fast, determined by the frequencies ω_γ and ω_ξ, respectively. Substituting the above decomposition for γ and ξ in the Lagrangian (2)–(4), and averaging over the fast variables $\delta\gamma$ and $\delta\xi$, we find the effective low-frequency potential energy

$$V(x,y,\psi) = 2E_J[-\cos(x)\cos(y) - s(\eta y + x) + b(y-y_B)^2] - E_{J1}^T \cos(\psi) - E_{J2}^T \cos[\psi - \xi_0(x,y) + \phi_T]. \quad (7)$$

Here we defined the reduced parameters $b = \phi_0/(LI_0)$, $s = I_b/(2I_0)$, and $y_B = \pi/(\Phi_S/\Phi_0)$. Furthermore, $E_J = \phi_0 I_0$, $E_{J1}^T = \phi_0 I_1^T$, and $E_{J2}^T = \phi_0 I_2^T$ are the different Josephson energies of the circuit. Note that the fast oscillations of ξ lead to a renormalization of I_2^T; the value it takes in the effective low-frequency potential (7) will therefore be smaller than the bare value appearing in (4). Assuming that the bias current I_b and the flux Φ_S are constant, we deduce from Eqs. (5) and (6) that $\dot{\gamma}_0 = \dot{x} + \eta\dot{y}$ and $\dot{\xi}_0 = \dot{x} - \eta\dot{y}$. The kinetic part of the Lagrangian can then be expressed as

$$T(\dot{x},\dot{y},\dot{\psi},\dot{\theta}) = \phi_0^2\{C_0\dot{x}^2 + C_0\dot{y}^2 + \tfrac{1}{2}C_2^T(\dot{x} - \eta\dot{y} - \dot{\psi})^2 + \tfrac{1}{2}C_1^T\dot{\psi}^2 + \tfrac{1}{2}C_g(\dot{\psi} - \dot{\theta})^2 + \tfrac{1}{2}C_P\dot{\theta}^2\}. \quad (8)$$

The four variables of the Lagrangian can be separated in three groups. Indeed, the dynamics of x and y corresponds to that of the dc SQUID, whereas the dynamics of ψ is associated with that of the ACPT. The variable θ is used to model the effect of the gate voltage (cf. Sec. II F). Note that the last term of the potential (7) and the third term of the kinetic term (8) couple the variables of the dc SQUID and those of the ACPT together, and therefore are responsible of the coupling between these two elements.

E. Choice of variables for the dc SQUID

The Lagrangian of the circuit is a function of the variables x and y associated with the SQUID. We want to change these variables to more appropriate ones which will be used below to describe the dynamics of the dc SQUID (cf. Sec. III). Let us introduce the two-dimensional potential of the dc SQUID $V_S(x,y)$, which is the contribution to the potential $V(x,y,\psi)$, Eq. (7), depending only on the variables x and y. It reads

$$V_S(x,y) = 2E_J[-\cos(x)\cos(y) - s(\eta y + x) + b(y-y_B)^2]. \quad (9)$$

We stress here that this potential is identical to the one of a dc SQUID alone, as studied by Claudon *et al.*[27] The dynamics of the dc SQUID is similar to that of a fictitious particle of mass $\approx \phi_0^2 2C_0$, which evolves in the potential $V_S(x,y)$. This potential undulates due to the product of cosine terms and contains wells that are separated by saddle points (see Fig. 3); $V_S(x,y)$ is modulated by the bias current I_b and the flux Φ_S. We consider now the case that the particle is trapped in one of these wells associated with a given local minimum (x_0,y_0). Let us introduce the displacement variables around (x_0,y_0) defined by $X = x - x_0$ and $Y = y - y_0$. We assume that the particle's motion does not extend far from (x_0,y_0). Then, we can replace the potential $V_S(x,y)$ by its third-order expansion around $(X=0, Y=0)$. This expansion contains a cross term in XY which disappears by performing a rotation of the (X,Y) plane [Fig. 3(b)] by the angle θ, where θ is given by $\tan(2\theta)/2 = \partial^2_{xy}U(x_0,y_0)/[\partial^2_{xx}U(x_0,y_0) - \partial^2_{yy}U(x_0,y_0)]$.

The new variables of the dc SQUID $X_\parallel$ and $Y_\perp$ associated with the rotated plane are defined by

$$\begin{pmatrix} X_\parallel \\ Y_\perp \end{pmatrix} = \begin{pmatrix} \cos(\theta) & \sin(\theta) \\ -\sin(\theta) & \cos(\theta) \end{pmatrix} \begin{pmatrix} X \\ Y \end{pmatrix}, \quad (10)$$

and correspond to the position of the particle along the longitudinal and the transverse direction, defined by the minimal and the maximal curvature of the potential, respectively. The successive changes of the dc SQUID variables are summarized in Table I.

The third-order expansion of the SQUID potential now takes the form

$$V_S(X_\parallel, Y_\perp) = \left[\tfrac{1}{2}k_\parallel X_\parallel^2 + \tilde{\sigma}_\parallel X_\parallel^3\right] + \left[\tfrac{1}{2}k_\perp Y_\perp^2 + \tilde{\sigma}_\perp Y_\perp^3\right] + [\beta_a Y_\perp^2 X_\parallel + \beta_b Y_\perp X_\parallel^2], \quad (11)$$

TABLE I. Successive changes of the dc SQUID variables. The first pair of variables are the node phases φ_1 and φ_2. The motion of the fictitious particle takes place around the local minimum (x_0,y_0) of the potential. The variables $X_\parallel$ and $Y_\perp$ correspond to the transversal and orthogonal displacement of this particle. θ is the angle between the axes X and $X_\parallel$ (see Fig. 3).

dc SQUID variables	
φ_1	φ_2
$x = (\varphi_1 + \varphi_2)/2$	$y = (\varphi_2 - \varphi_1)/2$
$X = x - x_0$	$Y = y - y_0$
$X_\parallel = \cos(\theta)X + \sin(\theta)Y$	$Y_\perp = -\sin(\theta)X + \cos(\theta)Y$

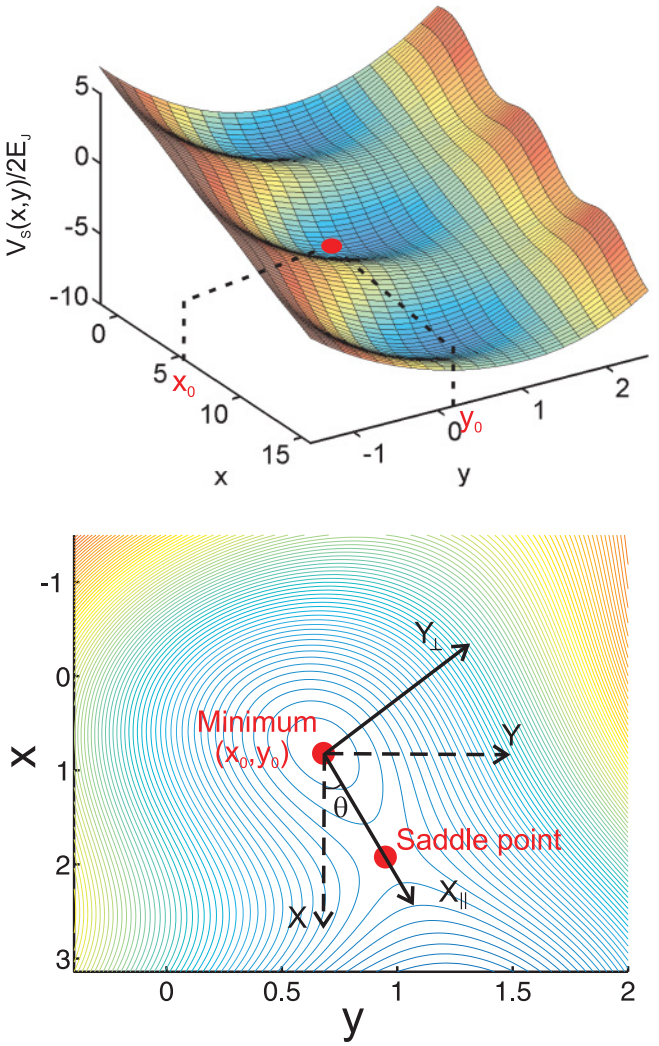

FIG. 3. (Color online) Potential $V_S(x,y)$ of the dc SQUID with bias parameters $s = 0.55$, $y_B = 0$ (SQUID parameters $b = 1.28$, $\eta = 0.29$). The point (x_0, y_0) is the local minimum of one of the potential wells.

where the prefactors $k_\parallel, \tilde{\sigma}_\parallel, k_\perp, \tilde{\sigma}_\perp, \beta_a$, and β_b can be calculated numerically. The dynamics of the fictitious particle of the SQUID in this potential will be analyzed in Sec. III. The full potential appearing in the Lagrangian, Eq. (7), is given by

$$\begin{aligned} V(X_\parallel, Y_\perp, \psi) = &\left[\tfrac{1}{2}k_\parallel X_\parallel^2 + \tilde{\sigma}_\parallel X_\parallel^3\right] + \left[\tfrac{1}{2}k_\perp Y_\perp^2 + \tilde{\sigma}_\perp Y_\perp^3\right] \\ &+ \left[\beta_a Y_\perp^2 X_\parallel + \beta_b Y_\perp X_\parallel^2\right] \\ &- E_{J1}^T \cos(\psi) - E_{J2}^T \cos(\hat{\psi} - \delta) \\ &- E_{J2}^T \alpha_\parallel \hat{X}_\parallel \sin(\hat{\psi} - \delta) + E_{J2}^T \alpha_\perp \hat{Y}_\perp \sin(\hat{\psi} - \delta), \end{aligned} \tag{12}$$

where $\delta \equiv \xi(x_0, y_0) - \phi_T$ is the classical phase difference across the transistor. The prefactors $\alpha_\parallel \equiv \cos(\theta) - \eta \sin(\theta)$ and $\alpha_\perp \equiv \sin(\theta) + \eta \cos(\theta)$ reflect the two dimensionality of the SQUID potential. When the inductance L_S is zero, the dynamics of the SQUID is described by only one variable, x, since $y = y_B$. In that case, the prefactors $\alpha_\parallel$ and $\alpha_\perp$ are equal to one. The two last terms of the potential contain one variable of the SQUID and one of the transistor. They thus couple the SQUID and the transistor. Note that the coupling terms of the second order and beyond have been neglected in the potential. The kinetic term of the Lagrangian can be rewritten as, using the variables $X_\parallel$ and $Y_\perp$,

$$\begin{aligned} T(\dot{X}_\parallel, \dot{Y}_\perp, \dot{\psi}, \dot{\theta}) = &\tfrac{1}{2}\phi_0^2 \left\{ \left(2C_0 + \alpha_\parallel^2 C_2^T\right) \dot{X}_\parallel^2 + \left(2C_0 + \alpha_\perp^2 C_2^T\right) \dot{Y}_\perp^2 \right. \\ &+ C_\Sigma \dot{\psi}^2 - 2C_2^T (\alpha_\parallel \dot{X}_\parallel - \alpha_\perp \dot{Y}_\perp) \dot{\psi} \\ &\left. - 2C_2^T \alpha_\parallel \alpha_\perp \dot{X}_\parallel \dot{Y}_\perp - 2C_g \dot{\psi}\dot{\theta} + (C_P + C_g)\dot{\theta}^2 \right\}, \end{aligned} \tag{13}$$

where C_Σ is the total capacitor of the transistor, defined by $C_\Sigma = C_1^T + C_2^T + C_g$. The final expression for the total Lagrangian is obtained from $\mathcal{L}(\dot{X}_\parallel, \dot{Y}_\perp, \dot{\psi}, \dot{\theta}, X_\parallel, Y_\perp, \psi) = T(\dot{X}_\parallel, \dot{Y}_\perp, \dot{\psi}, \dot{\theta}) - V(X_\parallel, Y_\perp, \psi)$; it will be used in the next section to establish the Hamiltonian of the circuit.

F. The Hamiltonian

The Hamiltonian of the coupled circuit is a function of the variables $(X_\parallel, Y_\perp, \psi, \theta)$ and the conjugate momenta $(-\hbar P_\parallel, -\hbar P_\perp, -\hbar n, -\hbar n_Q)$. These momenta are related to the velocities $(\dot{X}_\parallel, \dot{Y}_\perp, \dot{\psi}, \dot{\theta})$ by the well-known expressions $-\hbar P_\parallel \equiv \partial\mathcal{L}/\partial\dot{X}_\parallel$, $-\hbar P_\perp \equiv \partial\mathcal{L}/\partial\dot{Y}_\perp$, $-\hbar n \equiv \partial\mathcal{L}/\partial\dot{\Psi}$, and $-\hbar n_Q \equiv \partial\mathcal{L}/\partial\dot{\theta}$. The analytical expressions for the conjugate momentum variables are given in Appendix C. The conjugate variables generate the charges $P_\parallel$, n, and n_Q with unit $[-2e]$. We stress that these charges have a clear physical meaning. Indeed, $P_\parallel$ corresponds to the number of Cooper pairs stored in the two capacitors C_0; n is the number of Cooper pairs on the island. In Eq. (C4), the charge $-2en_Q$ is equal to the bias charge Q_b. Performing the limiting procedure $C_P, Q_b \to \infty$, keeping their ratio constant $Q_b/C_P = V_g$, we see that the velocity $\dot{\theta}$ is constant and defined by $\dot{\theta} = V_g/\phi_0$. The expression for the Hamiltonian is determined by the Legendre transformation[25]

$$\mathcal{H} = -\hbar P_\parallel \dot{X}_\parallel - \hbar P_\perp \dot{Y}_\perp - \hbar n \dot{\psi} - \mathcal{L}. \tag{14}$$

All the velocities which appear in the Lagrangian have to be replaced by the conjugate variables, inverting the set of equations given in Appendix C. The full Hamiltonian of the circuit then takes the form

$$\begin{aligned} &\widehat{H}(\widetilde{P}_\parallel, \widetilde{X}_\parallel, \widetilde{P}_\perp, \widetilde{Y}_\perp, \hat{n}, \hat{\psi}) \\ &= \frac{(2e)^2}{2C_\parallel}\widetilde{P}_\parallel^2 + \frac{1}{2}k_\parallel \widetilde{X}_\parallel^2 + \tilde{\sigma}\widetilde{X}_\parallel^3 + \frac{(2e)^2}{2C_\perp}\widetilde{P}_\perp^2 \\ &\quad + \frac{1}{2}k_\perp \widetilde{Y}_\perp^2 + \tilde{\sigma}_\perp \widetilde{Y}_\perp^3 + \frac{(2e)^2}{C_{\parallel\perp}}\widetilde{P}_\parallel \widetilde{P}_\perp + \beta_a \widetilde{Y}_\perp^2 \widetilde{X}_\parallel \\ &\quad + \beta_b \widetilde{Y}_\perp \widetilde{X}_\parallel^2 + \frac{(2e)^2}{2C_T}\left(\hat{n} - \frac{C_g V_g}{2e}\right)^2 \\ &\quad - E_{J1}^T \cos(\hat{\psi}) - E_{J2}^T \cos(\hat{\psi} - \delta) \\ &\quad + \frac{(2e)^2}{C_{n\parallel}}\widetilde{P}_\parallel\left(\hat{n} - \frac{C_g V_g}{2e}\right) - E_{J2}^T \alpha_\parallel \widetilde{X}_\parallel \sin(\hat{\psi} - \delta) \\ &\quad - \frac{(2e)^2}{C_{n\perp}}\widetilde{P}_\perp\left(\hat{n} - \frac{C_g V_g}{2e}\right) + E_{J2}^T \alpha_\perp \widetilde{Y}_\perp \sin(\hat{\psi} - \delta), \end{aligned} \tag{15}$$

TABLE II. Analytical expressions for the capacitances present in Hamiltonian (15) and the approximated expressions in the limit of $C_g \ll C_2^T$ and $C_1^T \ll C_0$. We have used the definitions $\tilde{C}^2 = 2C_0[C_\Sigma + C_R(1+\eta^2)]$, $C_\Sigma = C_1^T + C_2^T + C_g$, and $C_R = C_2^T(C_1^T + C_g)/2C_0$. The numerical values have been calculated for the parameters of the circuit studied in Ref. 17: $C_0 = 227$ fF, $C_1^T = 2.0$ fF, $C_2^T = 0.9$ fF, $C_g = 29$ aF, and for a zero escape angle ($\theta = 0$).

Capacitance labels	$C_\parallel$	$C_\perp$	C_T	$C_{n\parallel}$	$C_{n\perp}$	$C_{\parallel\perp}$
Exact expressions	$\frac{\tilde{C}^2}{C_\Sigma+\alpha_\perp C_R}$	$\frac{\tilde{C}^2}{C_\Sigma+\alpha_\parallel C_R}$	$\frac{\tilde{C}^2}{2C_0+C_2^T(1+\eta^2)}$	$\frac{\tilde{C}^2}{\alpha_\parallel C_2^T}$	$\frac{\tilde{C}^2}{(\alpha_\perp C_2^T)}$	$\frac{\tilde{C}^2}{(\alpha_\perp\alpha_\parallel C_R)}$
Approximated expressions	$2C_0$	$2C_0$	$C_1^T + C_2^T$	$\frac{2C_0(C_2^T+C_1^T)}{\alpha_\parallel C_2^T}$	$\frac{2C_0(C_2^T+C_1^T)}{\alpha_\perp C_2^T}$	$\frac{\tilde{C}^2}{\alpha_\perp\alpha_\parallel C_R}$
Numerical values	455.6 fF	455.1 fF	2.90 fF	653.0 fF	2.252 pF	1.17 nF

where the analytical expressions of the capacitances $C_\parallel$, $C_\perp$, C_T, $C_{n\parallel}$, $C_{n\perp}$, and $C_{\parallel\perp}$ are given in Table II. Applying the standard canonical quantization rules, the classical variables have been replaced by their corresponding quantum operators. The conjugate pairs satisfy the following commutation operations:

$$\begin{cases} [\widetilde{X}_\parallel, \widetilde{P}_\parallel] = -i, \\ [\widetilde{Y}_\perp, \widetilde{P}_\perp] = -i, \\ [\hat{\psi}, \hat{n}] = -i. \end{cases} \tag{16}$$

The properties of the Hamiltonian (15) are not trivial. It governs the quantum dynamics of three subsystems: the longitudinal and transverse phase oscillations within the dc SQUID and the charge dynamics of the ACPT. Moreover, the Hamiltonian describes the dominant coupling between the different quantum subsystems. Very complex dynamics can appear in this full circuit. In this paper we mainly concentrate on the dynamics of the longitudinal SQUID phase mode and the charge dynamics of the ACPT and as well as on their coupling. The next section is dedicated to the study of the dc SQUID Hamiltonian. We will deduce the simplified Hamiltonian for the longitudinal phase mode and justify why transverse phase mode can be neglected in this study.

III. dc SQUID

The dc SQUID potential has already been discussed in Sec. II E, where we introduced the change of the variables x and y to the variables $X_\parallel$ and $Y_\perp$. In this section, we first analyze the properties of the dc SQUID potential in more detail. Then, we investigate the Hamiltonian of the dc SQUID which is equivalent to that of a fictitious particle trapped in one of the wells of the potential. We will see under which conditions the dc SQUID behaves as a phase qubit. In this section, the coupling between the SQUID and the ACPT will be ignored such that we can consider the dc SQUID as an independent element.

A. dc SQUID potential

For an appropriate choice of bias parameters, i.e., the bias current I_b and the flux Φ_S, the SQUID potential contains wells that can be regrouped in families $[f]$.[28] The index f for the family $[f]$ is related to the number f of flux quanta trapped in the dc SQUID loop. The wells of the same family are located along the direction x, periodically spaced by a distance 2π, and separated by saddle points. Since these wells have exactly the same geometry, the physical properties of the SQUID are independent of the particular well in which the fictitious particle is localized. Wells of the family $[f]$ exist only if the bias current satisfies the relation $I_c^-[f] < I_b < I_c^+[f]$, where $I_c^+[f]$ and $I_c^-[f]$ are the positive and negative critical current of the family $[f]$, respectively. When $I_b = I_c^\pm[f]$, the local minima of the wells of the family $[f]$ and their closest saddle points coincide. The critical currents depend strongly on the flux Φ_S as shown in Fig. 4 for the experimental parameters of the circuit studied in Ref. 17. Here, for a given flux, the absolute values of the critical currents $I_c^+[f]$ and $I_c^-[f]$ are different. This difference originates from the finite inductance asymmetry of the dc SQUID ($\eta = 0.28$) and disappears when $\eta = 0$. For almost any value of the flux, the potential is characterized by a unique family of wells, except in the region close to $\pm\Phi_0/2$ where two families can coexist. This specific region has been investigated recently in order to study the double escape path of the particle, as well as to make the SQUID insensitive in first order to current fluctuations.[13] In the following we will discuss the Hamiltonian of the dc SQUID for the case where the fictitious particle is trapped in one of the wells of the potential.

B. Hamiltonian of the dc SQUID

In the full Hamiltonian (15) of the coupled circuit, we isolate the terms which only contain the operators $\widetilde{X}_\parallel$ and $\widetilde{Y}_\perp$ and their conjugate momenta $\widetilde{P}_\parallel$ and $\widetilde{P}_\perp$. These terms constitute the Hamiltonian of the dc SQUID

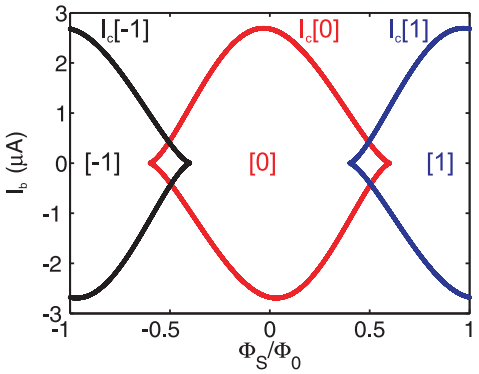

FIG. 4. (Color online) Critical current $I_c[f]$ for well family $[f]$ as a function of the flux Φ_S.

which takes the form

$$\begin{aligned}\widehat{H}_S = & E_C^{\parallel}\widetilde{P}_{\parallel}^2 + \frac{1}{2}k_{\parallel}\widetilde{X}_{\parallel}^2 + \tilde{\sigma}_{\parallel}\widetilde{X}_{\parallel}^3 \\ & + E_C^{\perp}\widetilde{P}_{\perp}^2 + \frac{1}{2}k_{\perp}\widetilde{Y}_{\perp}^2 + \tilde{\sigma}_{\perp}\widetilde{Y}_{\perp}^3 \\ & + \beta_a\widetilde{Y}_{\perp}^2\widetilde{X}_{\parallel} + \beta_b\widetilde{Y}_{\perp}\widetilde{X}_{\parallel}^2 + \frac{(2e)^2}{C_{\parallel\perp}}\widetilde{P}_{\parallel}\widetilde{P}_{\perp}, \end{aligned} \tag{17}$$

with the charging energies $E_C^{\parallel} = (2e)^2/(2C_{\parallel})$ and $E_C^{\perp} = (2e)^2/(2C_{\perp})$. The first three terms correspond to the Hamiltonian of a fictitious particle of mass $m = \phi_0^2 C_{\parallel}$ which is trapped in an anharmonic potential along the longitudinal direction $X_{\parallel}$. These terms govern the dynamics of an anharmonic oscillator of characteristic frequency $\nu_p = \sqrt{k_{\parallel}/m}/(2\pi)$. The next three terms correspond to the Hamiltonian of a fictitious particle of mass $m_{\perp} = \phi_0^2 C_{\perp}$ which is trapped in an anharmonic potential along the orthogonal direction $X_{\perp}$. These terms control the dynamics of an anharmonic oscillator of characteristic frequency $\nu_{\perp} = \sqrt{k_{\perp}/m_{\perp}}/(2\pi)$. The anharmonicity of the two oscillators is due to the cubic term which results from the nonlinearity of the JJ. The last three terms of the dc SQUID Hamiltonian mix the operators of the two oscillators and consequently couple them. Finally, the two-dimensional dynamics of the SQUID is similar to the dynamics of two coupled, one-dimensional oscillators. We proceed by introducing the following dimensionless operators: $\widehat{X}_{\parallel} = \sqrt{h\nu_p/2E_C^{\parallel}}\widetilde{X}_{\parallel}$, $\widehat{P}_{\parallel} = -\sqrt{2E_C^{\parallel}/h\nu_p}\widetilde{P}_{\parallel}$, $\widehat{Y}_{\perp} = \sqrt{h\nu_{\perp}/2E_C^{\perp}}\widetilde{Y}_{\perp}$, and $\widehat{P}_{\perp} = -\sqrt{2E_C^{\perp}/h\nu_{\perp}}\widetilde{P}_{\perp}$, which verify the commutation relations $[\widehat{X}_{\parallel}, \widehat{P}_{\parallel}] = i$ and $[\widehat{X}_{\perp}, \widehat{P}_{\perp}] = i$. With these new operators, the dc SQUID Hamiltonian can be rewritten as

$$\begin{aligned}\widehat{H}_S = & \tfrac{1}{2}h\nu_p(\widehat{P}_{\parallel}^2 + \widehat{X}_{\parallel}^2) - \sigma h\nu_p\widehat{X}_{\parallel}^3 \\ & + \tfrac{1}{2}h\nu_{\perp}(\widehat{P}_{\perp}^2 + \widehat{Y}_{\perp}^2) - \sigma_{\perp}h\nu_{\perp}\widehat{Y}_{\perp}^3 \\ & + h\nu_a^*\widehat{Y}_{\perp}^2\widehat{X}_{\parallel} + h\nu_b^*\widehat{Y}_{\perp}\widehat{X}_{\parallel}^2 + h\nu_c^*\widehat{P}_{\perp}\widehat{P}_{\parallel}, \end{aligned} \tag{18}$$

where the parameters σ and $\sigma_{\perp}$ correspond to the relative amplitude of the cubic term compared to the quadratic term and hence are direct measure of the degree of anharmonicity of the oscillators. The energies $h\nu_a^*, h\nu_b^*$, and $h\nu_c^*$ are the coupling energies between the two oscillators.

Hereafter, we suppose that the particle is trapped in one of the wells of the family [0]. The geometry of this well varies as a function of the bias point (I_b, Φ_S) of the circuit but does not change with the gate voltage V_g and the flux Φ_T. Therefore, the different parameters of the dc SQUID Hamiltonian only depend on I_b and Φ_S. Figure 5 shows numerical calculations of the parameters of the Hamiltonian under various biasing conditions, using the experimental parameters of the circuit studied in Ref. 17 (see Appendix B). Figures 5(a) and 5(b) show the dependence of the transverse (ν_p) and orthogonal ($\nu_{\perp}$) frequencies as a function of the bias point. Generally, the frequency $\nu_{\perp}$ is always higher than 35 GHz and is at least twice higher than ν_p. The frequency ν_p tends toward zero when the bias point approaches the critical current line. Figures 5(c)–5(e) show the dependence of the parameters of the Hamiltonian as a function of the flux Φ_S for a fixed bias current of 1.89 μA. Figure 5(d) shows the two anharmonicity parameters of the two oscillators. The anharmonicity σ is typically ~3% and increases close to the critical current line. The parameter $\sigma_{\perp}$ is very small regardless of the bias, which leads to us to the conclusion that the orthogonal oscillator can be considered as a harmonic one. Figure 5(e) shows the different coupling energies. The coupling frequency ν_c^* is of the order of 10 MHz and depends only weakly on Φ_S. The coupling frequencies ν_a^* and ν_b^* are generally much higher than ν_c^* and depend on Φ_S. Note that ν_b^* vanishes close to $\Phi_S = 0$ and ν_a^* is always negative. Numerical values of the parameters of the Hamiltonian, for $\Phi_S = 0.1\ \Phi_0$ and $I_b = 1.89\ \mu$A, are given in Table III. The energy ΔU of the potential barrier [Fig. 5(g)] corresponds to the energy which separates the local minimum of the well from its closest saddle point. This energy is not a parameter of the dc SQUID Hamiltonian (18). Nevertheless, if ΔU is sufficiently small, typically on the order of ν_p, expression (18) of $\widehat{H}_S$ is too simplified. This occurs when the bias point is close to the critical current line. One should then take into account the coupling of the quantum levels inside the well to those outside the well. Note that this coupling is responsible of the escape of the particle from the well.[30,31] This coupling will be neglected in the following, assuming that the particle is always trapped in a sufficiently deep well.

As $\nu_{\perp} \gg \nu_{\parallel}$, the quantum dynamics of the transverse oscillator is much faster than that of the longitudinal oscillator. We will assume in the following that the transverse oscillator is always in its ground state. It allows us to replace in $\widehat{H}_S$ (18) the operators of the transverse oscillator by their average values given by $\langle\widehat{Y}_{\perp}\rangle = 0$, $\langle\widehat{Y}_{\perp}^2\rangle = 1/2$, and $\langle\widehat{P}_{\perp}\rangle = 0$. Only one of the three coupling terms remains after this simplification. The coupling reads $h\nu_a^*\widehat{X}_{\parallel}/2$ and can be seen as a modification of the bias current I_b of less than 0.5 nA. This term will be neglected in the following. Under this condition, the dynamics of the particle along the longitudinal direction is given by the Hamiltonian

$$\widehat{H}_S = \tfrac{1}{2}h\nu_p w(\widehat{P}_{\parallel}^2 + \widehat{X}_{\parallel}^2) - \sigma h\nu_p\widehat{X}_{\parallel}^3. \tag{19}$$

In the following, the energy spectrum of the dc SQUID will be studied, using this simplified Hamiltonian.[30] We denote by $|n\rangle$ and E_n the eigenstates and the associated eigenenergies

TABLE III. Numerical values of the parameters of the dc SQUID Hamiltonian at the working point $\Phi_S = 0.1\ \Phi_0$ and $I_b = 1.89\ \mu$A, calculated using the experimental parameters of the circuit studied in Ref. 17.

Longitudinal oscillator		Transverse oscillator		Coupling		
ν_p	σ	$\nu_{\perp}$	$\sigma_{\perp}$	ν_a^*	ν_b^*	ν_c^*
16.24 GHz	3.4 %	38.26 GHz	−0.006 %	−612 MHz	−348 MHz	12 MHz

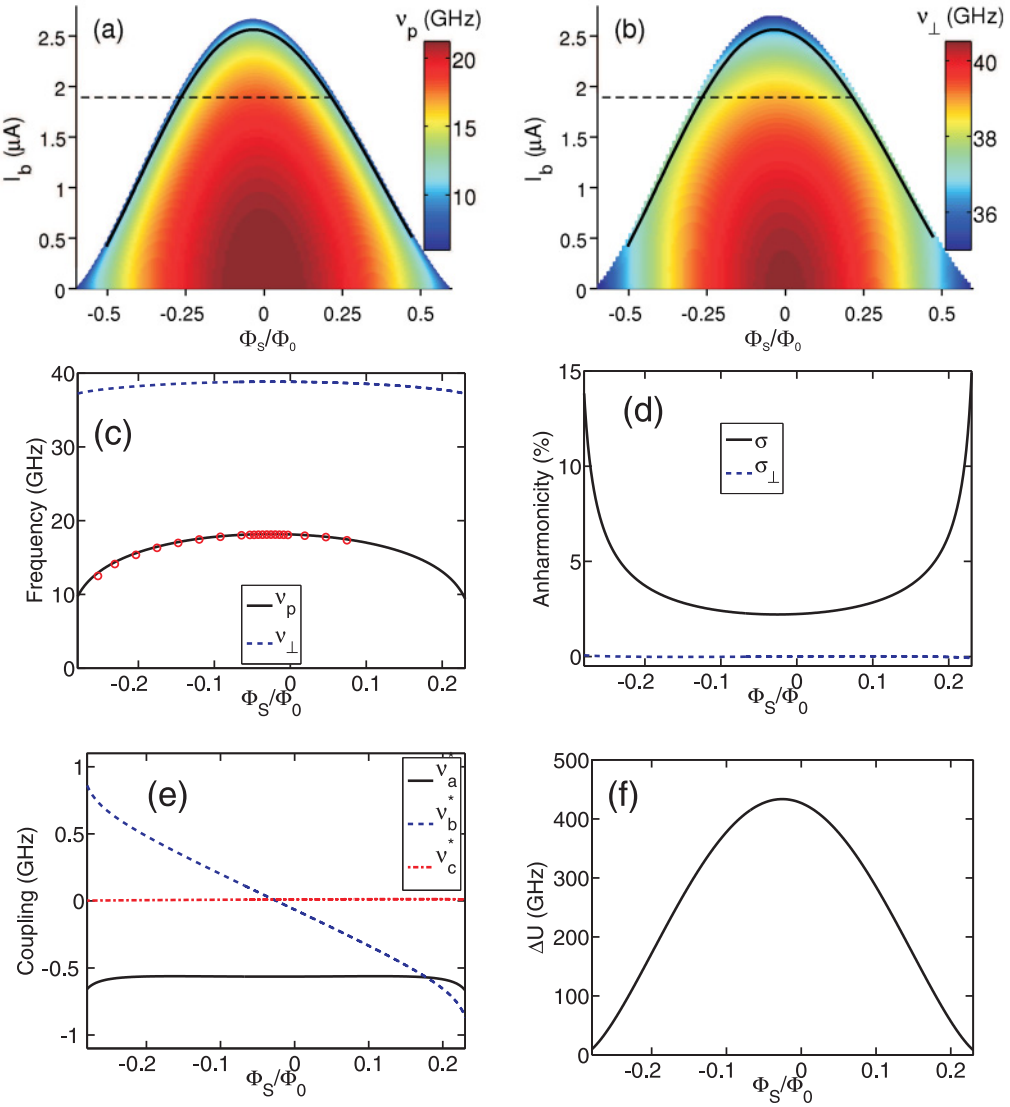

FIG. 5. (Color online) Numerical calculations of the parameters of the dc SQUID Hamiltonian (17), using the experimental parameters of the circuit studied in Ref. 17. The fictitious particle associated to the SQUID is trapped in a potential well of the family [0]. (a) Frequencies of the transverse and (b) orthogonal oscillators, i.e., ν_p and $\nu_\perp$, respectively, as a function of the flux Φ_S and the bias current I_b. The black line shows the measured switching current of the dc SQUID from Ref. 29, which is close to the critical current. (c) Frequencies ν_p and $\nu_\perp$ as a function of Φ_S for $I_b = 1.89$ μA, i.e., for the bias points located on the dashed line of (a) and (b). Measured frequencies ν_S from Ref. 29 are shown as red points. (d) Anharmonicity parameters σ and $\sigma_\perp$ of the longitudinal and orthogonal oscillators, respectively, as a function of Φ_S for $I_b = 1.89$ μA. (e) Different coupling frequencies ν_a^*, ν_b^*, and ν_c^* between the two oscillators associated with the terms in $\widehat{Y}_\perp^2\widehat{X}_\parallel$, $\widehat{Y}_\perp\widehat{X}_\parallel^2$, and $\widehat{P}_\perp\widehat{P}_\parallel$ of $\widehat{H}_S$ (17). (f) Energy ΔU for the potential barrier as a function of ϕ_S for $I_b = 1.89$ μA.

of $\widehat{H}_S$, respectively, such that $\widehat{H}_S|n\rangle = E_n|n\rangle$, where n is an integer number larger or equal to zero. If the anharmonicity is weak ($\sigma \ll 1$), the energies E_n are given by a straightforward perturbative calculation and we find $E_n = (n+1/2)h\nu_p - 15/4\sigma^2(n+1/2)^2h\nu_p$. Figure 6 shows the approximate potential of the dc SQUID and the three first eigenenergies. When the anharmonicity of the dc SQUID is sufficiently large, the dynamics of the dc SQUID in the presence of an external microwave perturbation involves only the two first levels $|0\rangle$ and $|1\rangle$.[27] In that case, the dc SQUID behaves as a qubit. Since for the dc SQUID the Josephson energy is much larger than the charging energy, the fluctuations of the phase $\widetilde{X}_\parallel$ are much smaller than those of the charge $\widetilde{P}_\parallel$. For this reason, the dc SQUID is referred to as a phase qubit.[13] The dc SQUID Hamiltonian can be rewritten in the basis $(|1\rangle,|0\rangle)$, using the Pauli matrices (see Appendix D), as $\widehat{H}_S = h\nu_s/2\sigma_z^S$, where $\nu_S \equiv (E_1 - E_0)/h$ is the characteristic qubit frequency. The frequency ν_S can be approximated in first order with respect to the anharmonicity σ as $h\nu_S = h\nu_p[1 - (15/2)\sigma^2]$. We see that the frequency ν_S equals the plasma frequency ν_p if the dc SQUID anharmonicity is zero and decreases with increasing anharmonicity [see Fig. 5(c)]. When the anharmonicity σ is zero, the dc SQUID behaves as a harmonic oscillator described by the typical Hamiltonian $\hat{H}_S = h\nu_p(\hat{a}\hat{a}^\dagger + 1/2)$, where $\hat{a}^\dagger$ and $\hat{a}$ are the one-plasmon creation and annihilation operators, respectively.

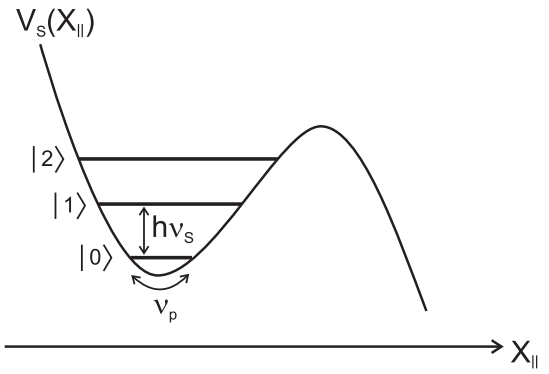

FIG. 6. Approximate one-dimensional potential of the dc SQUID in the direction $X_\parallel$. Eigenenergies of the first quantum states $|0\rangle$, $|1\rangle$, and $|2\rangle$.

IV. ASYMMETRIC COOPER PAIR TRANSISTOR (ACPT)

The dc SQUID Hamiltonian is only one of the terms that appear in the full Hamiltonian of the circuit. It is coupled to a second term associated with the ACPT. This section is dedicated to the theoretical analysis of the ACPT Hamiltonian, neglecting its coupling with the dc SQUID. We will first build and analyze the ACPT Hamiltonian and will show that the ACPT can be viewed as a charge qubit. We will then describe the ACPT by using only two charge states. The errors on the level of the eigenenergies and the eigenstates induced by this simplified description will be estimated.

A. ACPT Hamiltonian

The ACPT Hamiltonian is identified by isolating from the full Hamiltonian of the circuit (15), the terms which only contain the operators $\hat{\psi}$ and $\hat{n}$. After some straightforward algebra, the ACPT Hamiltonian reads

$$\hat{H}_{\rm ACPT} = E_C^T(\hat{n}-n_g)^2 - E_J^T\cos(\delta/2)\cos(\hat{\psi}-\delta/2) + \mu\sin(\delta/2)\sin[\hat{\psi}-\delta/2)], \quad (20)$$

where $E_J^T \equiv E_{J1}^T + E_{J2}^T$ and $E_C^T \equiv (2e)^2/(2C_T)$ are the Josephson and charging energies of the ACPT, respectively. It is the generalization of the quantronium Hamiltonian[15] for which asymmetries in critical current and capacitance of the Cooper pair transistor were neglected. The gate charge $n_g \equiv C_g V_g/(2e)$ corresponds to the number of Cooper pairs induced by the voltage applied to the gate capacitance. The charge states $|n_{2e}\rangle$ are the eigenvectors of the charge operator $\hat{n}$, such $\hat{n}|n_{2e}\rangle = n|n_{2e}\rangle$, where $n = 0, \pm 1, \pm 2\ldots$ is the number of excess Cooper pairs on the transistor island. Using the commutation relation $[\hat{\psi},\hat{n}] = i$, we identify the action of the operator $e^{i\hat{\psi}} = \sum_n |n_{2e}\rangle\langle(n+1)_{2e}|$, which decreases the number of Cooper pairs on the island by one unit. In the charge representation, the ACPT Hamiltonian can be written as

$$\hat{H}_{\rm ACPT} = E_C^T(\hat{n}-n_g)^2 - \frac{\rho_j(\delta)}{2}\left[\sum_n e^{-i(\delta/2+\chi)}|n_{2e}\rangle\langle(n+1)_{2e}| + \sum_n e^{i(\delta/2+\chi)}|(n+1)_{2e}\rangle\langle n_{2e}|\right], \quad (21)$$

with $E_J^T/2[\cos(\delta/2) + i\mu\sin(\delta/2)] \equiv \rho_j(\delta)/2e^{i\chi}$, $\tan\chi = \mu\tan(\delta/2)$, and $\rho_j(\delta)^2 = {E_J^T}^2[\cos^2(\delta/2) + \mu^2\sin^2(\delta/2)]$. The ACPT Hamiltonian is composed of a charging and a Josephson term which are proportional to E_C^T and $\rho_j(\delta)$, respectively. Let us focus first on the case of a zero Josephson coupling ($\rho_j = 0$). The eigenstates of the ACPT Hamiltonian are then the charge states $|n_{2e}\rangle$ with the associated eigenenergies $E_C^T(n-n_g)^2$. Figure 7 shows the energy spectrum of the ACPT as a function of n_g for a charging energy $E_C^T = 1.28$ K. This spectrum consists of a series of parabolas, each parabola being associated with a specific charge state $|n_{2e}\rangle$ with a minimum energy for $n_g = n$. Notice that when the energy difference between the ground charge state and the first excited charge state is much larger than $k_B T$, the charge on the island is well quantized leading to the Coulomb blockade phenomena.[32] For $n_g = 0.5$, the energy parabolas of the states $|0_{2e}\rangle$ and $|1_{2e}\rangle$ cross each other and the states $|0_{2e}\rangle$ and $|1_{2e}\rangle$ are degenerate. This degeneracy is lifted by the Josephson term which couples the neighboring charge states to each other. The amplitude of this Josephson coupling is given by ρ_j. Figure 8 shows the dependence of ρ_j on δ for three different Josephson asymmetries. Since ρ_j is 2π periodic in δ, the range of δ has been restricted to the interval between -2π and 2π. In the case of a symmetric transistor ($\mu = 0$), the Josephson coupling is maximum for $\delta = 0$, equal to E_J^T; it is zero at $\delta = \pm\pi$. For a finite asymmetry μ, the Josephson coupling reaches a maximum for $\delta = 0$ and equals E_J^T, and a minimum equals to μE_J^T for $\delta = \pm\pi$. For a Cooper pair box ($\mu = \pm 100\%$), the Josephson coupling does not depend on δ and remains equal to E_J^T. The Josephson coupling then depends strongly on the Josephson asymmetry, especially for $\delta = \pm\pi$, where it can vary from zero to E_J^T. The full energy spectrum of the ACPT, which takes into account the Josephson coupling, is calculated numerically by diagonalizing the Hamiltonian (21) with eight charge states. It is plotted as a function of n_g in Fig. 7 for a fixed superconducting phase $\delta = 0$ and for the parameters of Ref. 17: $E_C^T = 1.28$ K, $E_J^T = 1.01$ K and $\mu = -41.6\%$. The spectrum consists of several energy bands which do not cross each other, leading to an energy gap between the lowest and the first bands. We associate with these two bands the ground state $|-\rangle$ and the first excited state $|+\rangle$, respectively. These two states correspond to the states of a qubit, with a characteristic energy $h\nu_T$. Note that to operate the ACPT as a qubit, the gate charge should be close to 0.5 (modulo 1) where the transition energy from the state $|+\rangle$ to the third level is higher than the frequency ν_T. Indeed, when the ACPT Hamiltonian (21) is subject to an adequate perturbation, the quantum dynamics of the ACPT will only involve the states $|-\rangle$ and $|+\rangle$. Because $E_J^T > E_C^T$, the states $|-\rangle$ and $|+\rangle$ can be written as a superposition of a few charge states (typically four). For this reason, the qubit formed by the ACPT is referred to as a charge qubit. The Hamiltonian of the charge qubit can be written using the Pauli matrix (see Appendix D) as

$$\frac{h\nu_T}{2}\hat{\sigma}_z^T. \quad (22)$$

The frequency ν_T of the charge qubit depends on the two parameters δ and n_g as shown in Fig. 9(a). This frequency, as is ρ_j, is also 2π periodic as a function of δ. It is maximum and minimum at the points ($\delta = 0, n_g = 1/2$) and ($\delta = \pi, n_g =$

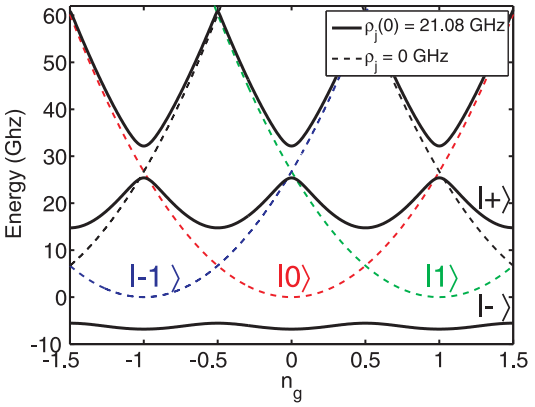

FIG. 7. (Color online) Energy spectrum of the ACPT as a function of n_g in the case of a zero Josephson coupling (dashed lines) and in the case of $\rho_j(\delta = 0) = 21.08$ GHz (full lines). These energy spectra have been calculated numerically, using the parameters from Ref. 17: $E_J^T = 21.08$ GHz, $E_C^T = 26.76$ GHz, and $\mu = -41.6\%$. The states $|-\rangle$ and $|+\rangle$ associated to the two lowest-energy bands correspond to the states of the charge qubit.

1/2), respectively. These are optimal points where the ACPT is, in first order, insensitive to charge, flux and current fluctuations. Figure 10 shows the experimental frequency of the charge qubit measured in Ref. 17 as a function of δ. The theoretical fit, shown in red, is obtained by diagonalizing the ACPT Hamiltonian (21) in a basis of eight charge states. It allows us to accurately find the parameters of the charge qubit, i.e., the Josephson energy $E_J^T = 21.08$ GHz, the charging energy $E_C^T = 26.76$ GHz, and the Josephson asymmetry $\mu = -41.6\%$. Nevertheless, the capacitance asymmetry can not be extracted from the fit since it does not enter in the ACPT Hamiltonian (21). The Josephson energy and the capacitance of a JJ of the ACPT are both proportional to the junction surface and, therefore, the capacitance and Josephson asymmetries are equal in first approximation. We will see in Sec. V that the capacitance asymmetry can be extracted from the coupling between the dc SQUID and the ACPT and we will find $\lambda = 0.875\mu$.

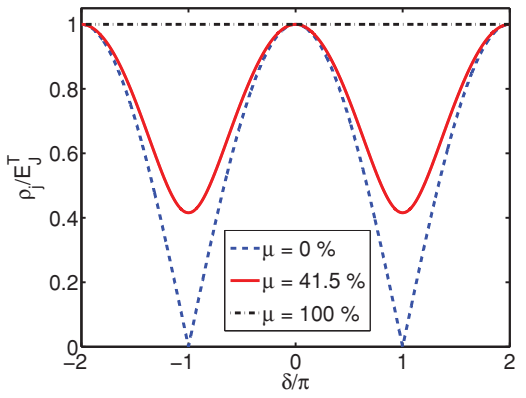

FIG. 8. (Color online) Josephson coupling ρ_j as a function of the superconducting phase δ across the ACPT, for three different Josephson asymmetries: $\mu = 0$ for a symmetric transistor, $\mu = -41.5\%$ for an asymmetric transistor, and $\mu = 100\%$ for a Cooper pair box.

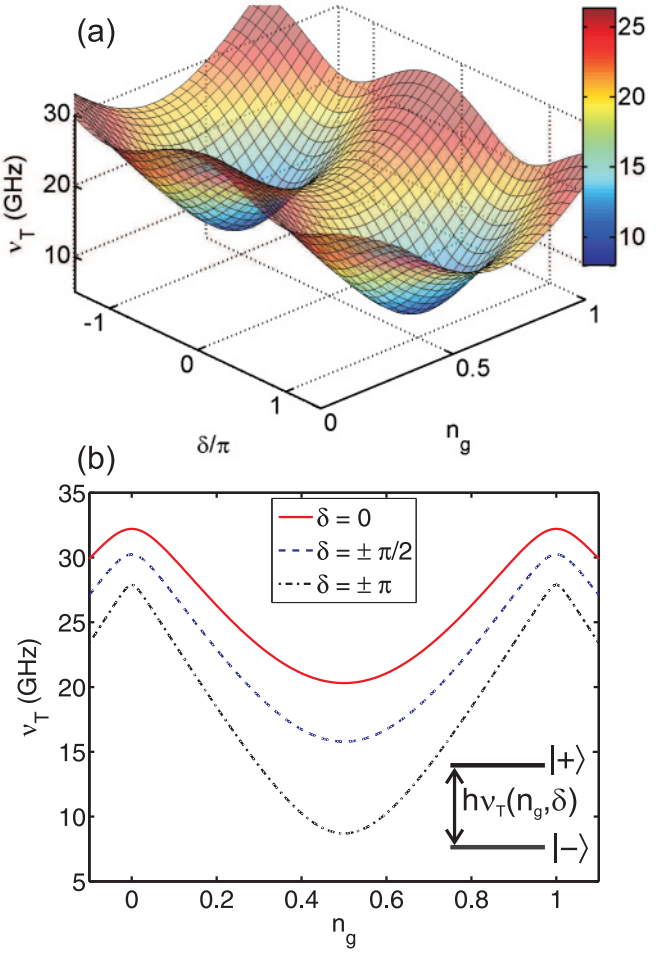

FIG. 9. (Color online) (a) Frequency ν_T of the charge qubit as a function of n_g and δ for the experimental parameters of Ref. 17: $E_C^T = 1.28 k_B$ K, $E_J^T = 1.01 k_B$ K, and $\mu = -41.6\%$. (b) Frequency ν_T as a function of n_g for $\delta = 0$, $\delta = \pm\pi/2$, and $\delta = \pi$.

B. Description of the ACPT with two charge levels

If the Josephson coupling ρ_j is much smaller than the charging energy E_C^T and if $n_g \approx 0.5$, the qubit states can be expressed as a superposition of the two charge states $|0_{2e}\rangle$ and $|1_{2e}\rangle$. In that case, the Hamiltonian of the transistor is simply given by its matrix form $\hat{H}^0_{\rm ACPT}$, which reads, in the charge basis $(|0_{2e}\rangle,|1_{2e}\rangle)$,

$$\hat{H}^0_{\rm ACPT} = \begin{pmatrix} E_C^T n_g^2 & -\rho_j e^{-i(\delta/2+\chi)}/2 \\ -\rho_j e^{i(\delta/2+\chi)}/2 & E_C^T(1-n_g)^2 \end{pmatrix}. \quad (23)$$

The eigenvalues of this simplified Hamiltonian are given by $E^0_\pm = \frac{1}{2}E_C^T[n_g^2 + (1-n_g)^2] \pm \frac{1}{2}\sqrt{E_C^{T\,2}(1-2n_g)^2 + \rho_j^2}$, and the qubit energy reads $h\nu_T^0 = E^0_+ - E^0_-$. Note that for $n_g = 0.5$, we have $h\nu_T^0 = \rho_j$. The eigenstates $|-_0\rangle$ and $|+_0\rangle$, associated with the energies E_- and E_+, can be written as a function of the charge states as

$$\begin{cases} |+_0\rangle = \alpha^*|0_{2e}\rangle + \beta|1_{2e}\rangle, \\ |-_0\rangle = -\beta^*|0_{2e}\rangle + \alpha|1_{2e}\rangle, \end{cases} \quad (24)$$

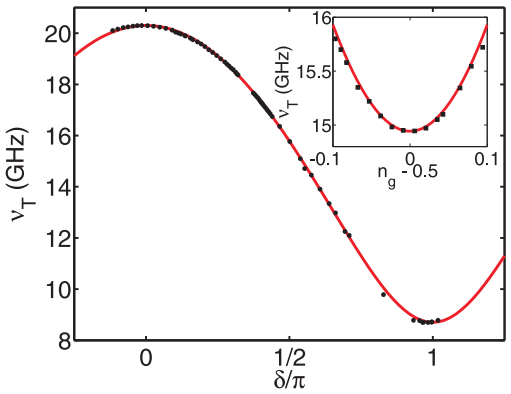

FIG. 10. (Color online) Frequency ν_T as a function of the phase δ. The points are the experimental data from Ref. 17. The solid curve is the theoretical frequency ν_T calculated by diagonalizing the ACPT Hamiltonian (21) with the parameters $E_J^T = 21.08$ GHz, $E_C^T = 26.76$ GHz, and $\mu = -41.6\%$. Inset: Frequency ν_T as a function of n_g for $\delta = 0.549\pi$. The points are the experimental frequencies ν_T and the solid line is the theoretical frequency ν_T calculated as before.

with $\alpha = \cos(\theta/2)e^{i(\delta/2+\chi-\pi)/2}$, $\beta = \sin(\theta/2)e^{i(\delta/2+\chi-\pi)/2}$, and $\tan\theta = -\frac{2|\rho_j|}{E_C^T(1-2n_g)}$ ($\theta \in [0,\pi]$).

For the ACPT studied experimentally in Ref. 17, the condition $\rho_j(\delta) \ll E_C^T$ is too strong, especially at $\delta = 0$ where the ratio $\rho_j/E_C^T \approx 79\%$ is maximum. For this reason, we would like to quantify the error induced by the description of the ACPT with only two charge states. Let us first focus on the error in the qubit energy. Figure 11 shows the difference between the frequencies ν_T^0 calculated with two charge states and the real frequency ν_T as a function of δ for $n_g = 0.5$. This difference is minimum for $\delta = \pm\pi$ and equals 58 MHz, corresponding to an error in energy of 0.5%. For $\delta = 0$, the difference is maximum and equals 780 MHz, corresponding to an error in energy of 3.8%.

We now discuss the error made on the level of the states $|-_0\rangle$ and $|+_0\rangle$. The nonreduced Hamiltonian of the ACPT can be rewritten as a function of $\widehat{H}^0_{\rm ACPT}$ as $\widehat{H}_{\rm ACPT} = \widehat{H}^0_{\rm ACPT} + \widehat{W}$, where $\widehat{W}$ is a perturbative term which takes the form

$$\widehat{W} = -\frac{\rho_j(\delta)}{2}\sum_{n\neq 0}[e^{-i(\delta/2+\chi)}|n\rangle\langle n+1| + e^{i(\delta/2+\chi)}|n+1\rangle\langle n|] + E_C^T\sum_{n\neq\{0,1\}}(n-n_g)^2|n\rangle\langle n|.$$

Using first-order perturbation theory, we calculate the probability $|\langle -_0|-\rangle|^2$ ($|\langle +_0|+\rangle|^2$) that the state $|-\rangle$ ($|+\rangle$) is in the the state $|-_0\rangle$ ($|+_0\rangle$). Figure 11 shows the dependence of these probabilities as a function of δ for $n_g = 0.5$. The probability $|\langle -_0|-\rangle|^2$ is always smaller than the probability $|\langle +_0|+\rangle|^2$. Indeed, the energy of the state $|+_0\rangle$ is closer to the charging energies of the states $|-1_{2e}\rangle$ and $|2_{2e}\rangle$ and consequently more perturbed by these two states. The probabilities are minimum for $\delta = 0$ ($|\langle -_0|-\rangle|^2 = 97.4\%$ and $|\langle -_0|-\rangle|^2 = 94.7\%$) and, therefore, for this value of the phase, the error made by considering the states of the ACPT as $|-_0\rangle$ and $|+_0\rangle$ is maximum. Figure 11 shows the dependence of the probabilities $|\langle -_0|-\rangle|^2$ and $|\langle +_0|+\rangle|^2$ as a function of the ratio

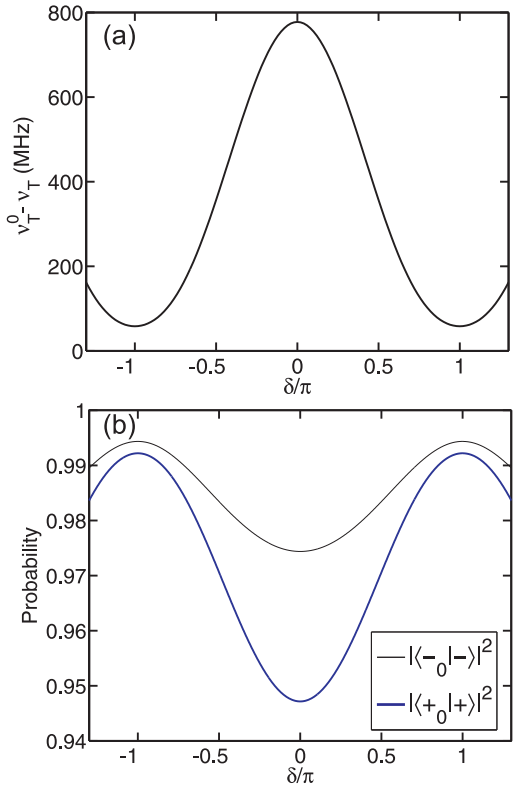

FIG. 11. (Color online) Errors in the energies and states of the charge qubit of Ref. 17 induced by describing it with only two charge states. (a) Difference between the qubit frequency ν_T^0 calculated with two charge states and its real frequency ν_T as a function of δ for $n_g = 0.5$. (b) Probabilities $|\langle -_0|-\rangle|^2$ (black) and $|\langle +_0|+\rangle|^2$ (blue) as a function of δ for $n_g = 0.5$.

E_J^T/E_C^T for $\delta = 0$. Theses probabilities have been calculated with a first-order perturbation theory and also numerically by using eight charge states. We see that when $E_J^T/E_C^T < 1$, the first-order perturbation theory agrees quite well with the numerical simulations. But when $E_J^T/E_C^T > 1$, the analytical calculation gives probabilities significantly lower than the numerical one. The probabilities $|\langle -_0|-\rangle|^2$ and $|\langle +_0|+\rangle|^2$ decrease with increasing E_J^T/E_C^T, which is explained by the fact that the Josephson coupling mixes more and more the charge states $|0_{2e}\rangle$ and $|1_{2e}\rangle$ with the other, closer-in-energy charge states. In order to simplify the calculation of the analytical expression of the coupling (see below), we consider in the following that $|-\rangle = |-_0\rangle$ and $|+\rangle = |+_0\rangle$, but do not approximate the qubit frequency to ν_T^0.

V. COUPLING

So far, we have considered independently the Hamiltonian of the longitudinal mode of the dc SQUID and the ACPT. However, in the studied circuit the dc SQUID and the ACPT are connected in parallel and therefore coupled to each other. The independence of the ACPT and the dc SQUID has to be reconsidered especially when the two qubits are close to resonance ($\nu_S \approx \nu_T$). In this case the coupling effects are the strongest. In this section, we derive the expression of the coupling Hamiltonian by considering the ACPT as a charge qubit and the dc SQUID as either a tunable harmonic oscillator

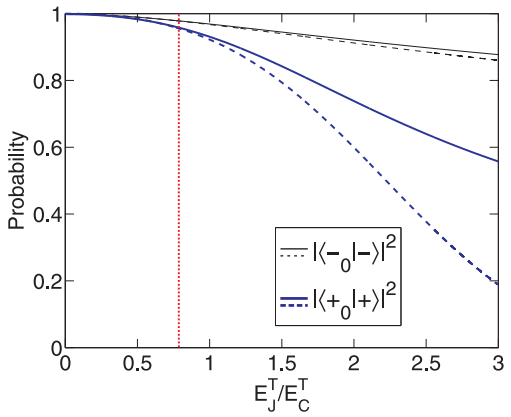

FIG. 12. (Color online) Probabilities $|\langle -_0|-\rangle|^2$ (black) and $|\langle +_0|+\rangle|^2$ (blue) as a function of the ratio E_J^T/E_C^T for $n_g = 0.5$ and $\delta = 0$. Numerical calculations of these probabilities (full lines) are compared with first-order perturbation calculations (dashed lines). The vertical dashed line indicates the values of these probabilities at the ratio $E_J^T/E_C^T = 79\%$ corresponding to those of the ACPT studied in Ref. 17.

or a phase qubit. We will see that the total coupling is the sum of two distinct contributions: a capacitive and an inductive Josephson coupling.

A. Capacitive coupling

The capacitive coupling Hamiltonian couples by definition the charge of the dc SQUID with that of the ACPT. It reads

$$\hat{H}_{\text{Coupl,Capa}} = -\frac{(2e)^2}{C_{n\|}}\sqrt{\frac{h\nu_p}{2E_C^{\|}}}\,\widehat{P}_{\|}(\hat{n} - n_g). \tag{25}$$

We consider hereafter two different limits for the dc SQUID in order to simplify this capacitive coupling Hamiltonian.

The first limit corresponds to a dc SQUID with an anharmonicity factor σ equal to zero. This limit can be achieved when the fictitious particle associated with the dc SQUID is trapped in a deep well, which is generally true when the dc SQUID is biased at the working point $I_b = 0$ and $\Phi_S = 0$. Under this condition, the dc SQUID behaves as a harmonic oscillator and several levels are involved in the dynamics. The momentum operator in the charge coupling Hamiltonian is then given by $\widehat{P}_{\|} = (\hat{a}^\dagger + \hat{a})/\sqrt{2}$, where $\hat{a}^\dagger$ and $\hat{a}$ are the one-plasmon creation and annihilation operators. If we describe the charge qubit with two charge states [Eq. (24)], the operator $\hat{n}$ can be written as $\widehat{n} = \frac{1}{2}\hat{I} + \frac{1}{2}\sin(\theta)\hat{\sigma}_x^T - \frac{1}{2}\cos(\theta)\hat{\sigma}_z^T$, where $\hat{I}$ is the identity operator and σ_x^T and σ_y^T are the Pauli matrices defined in the eigenstate basis of the charge qubit. For $n_g = 1/2$, we have $\theta = \pi/2$ and the charge coupling Hamiltonian simplifies to

$$\widehat{H}_{\text{Coupl,Capa}} = -E_{c,c}(\hat{a}^\dagger + \hat{a})\hat{\sigma}_x^T, \tag{26}$$

where $E_{c,c} = e^2\sqrt{h\nu_p/E_C^{\|}}/C_{n\|}$ determines the strength of the capacitive coupling.

The second limit is realized when the anhamonicity σ is typically $\sim$3% or larger; then the dc SQUID can be described as a phase qubit. Generally, σ does not exceed 10% [see Fig. 5(d)] so the two lowest eigenstates of the dc SQUID Hamiltonian are very close to the two lowest eigenstates of the harmonic oscillator. Consequently, the momentum operator can be expressed in terms of the eigenbasis of the phase qubit as $\widehat{P}_{\|} \approx (|0\rangle\langle 1| + |1\rangle\langle 0|)/\sqrt{2} = \hat{\sigma}_x^S/\sqrt{2}$. For $n_g = 1/2$, the charge coupling Hamiltonian takes the following form:

$$\widehat{H}_{\text{Coupl,Capa}} = -E_{c,c}\hat{\sigma}_x^S\hat{\sigma}_x^T. \tag{27}$$

The capacitive coupling produces a transverse interaction between the two quantum systems. This coupling was already discussed in Refs. 33 and 34 where a Cooper pair box was coupled to a harmonic oscillator. The capacitive coupling is vanishing in the limit of small C_2^T. We notice also that $E_{c,c}$ depends on the bias variables through $\sqrt{\nu_p}$ and therefore is weakly tunable.

B. Josephson coupling

The Josephson coupling Hamiltonian couples the phases $\widehat{X}_{\|}$ and $\hat{\psi}$ associated with the dc -SQUID and the transistor, respectively. This coupling is mediated via the JJ 2 of the ACPT and reads

$$\hat{H}_{\text{Coupl,Jos}} = -E_{J2}^T\alpha_{\|}\sqrt{\frac{2E_C^{\|}}{h\nu_p}}\,\widehat{X}_{\|}\sin(\hat{\psi} - \delta). \tag{28}$$

We derive now the expression of the Josephson coupling Hamiltonian for the two different limits of the dc SQUID. When the dc SQUID is in the harmonic oscillator limit, the position operator can be written as $\widehat{X}_{\|} = i(\hat{a} - \hat{a}^\dagger)/\sqrt{2}$. On the other hand, close to $n_g = 1/2$, the operator $\sin(\widehat{\psi} - \delta)$ takes the following form in the charge basis: $\sin(\widehat{\psi} - \delta) = \frac{i}{2}(e^{i\delta}|1_{2e}\rangle\langle 0_{2e}| - e^{-i\delta}|0_{2e}\rangle\langle 1_{2e}|)$. Using Eq. (24), the Josephson coupling Hamiltonian becomes

$$\begin{aligned}\widehat{H}_{\text{Coupl,Jos}} = -iE_{c,j}(\hat{a} - \hat{a}^\dagger)\big\{\sin(\delta/2 - \chi)\big[\sin(\theta)\hat{\sigma}_z^T \\ + \cos(\theta)\hat{\sigma}_x^T\big] - \cos(\delta/2 - \chi)\hat{\sigma}_y^T\big\},\end{aligned} \tag{29}$$

where $E_{c,j} = \alpha_{\|}/2E_{J2}^T\sqrt{E_C^{\|}/h\nu_p}$ quantifies the strength of the Josephson coupling. For $n_g = 0.5$, we have $\theta = \pi/2$ and the Josephson coupling Hamiltonian reduces to

$$\begin{aligned}\widehat{H}_{\text{Coupl,Jos}} = iE_{c,j}(\hat{a} - \hat{a}^\dagger)\big[\cos(\delta/2 - \chi)\hat{\sigma}_y^T \\ - \sin(\delta/2 - \chi)\hat{\sigma}_z^T\big].\end{aligned} \tag{30}$$

In the limit of finite anharmonicity σ, the dc SQUID can be approximated by a two-level system. In that case, the position operator can be written in the eigenbasis of the phase qubit as $\widehat{X}_{\|} \approx i(|0\rangle\langle 1| - |1\rangle\langle 0|)/\sqrt{2} = \hat{\sigma}_y^S/\sqrt{2}$. Using the latter expression, the Josephson coupling between the charge and phase qubits takes the following form for $n_g = 1/2$:

$$\begin{aligned}\widehat{H}_{\text{Coupl,Jos}} = E_{c,j}\cos(\delta/2 - \chi)\hat{\sigma}_y^S\hat{\sigma}_y^T \\ -E_{c,j}\sin(\delta/2 - \chi)\hat{\sigma}_y^S\hat{\sigma}_z^T.\end{aligned} \tag{31}$$

The Josephson coupling contains two different terms. One describes a transverse coupling $\hat{\sigma}_y^S\hat{\sigma}_y^T$ or $(\hat{a} - \hat{a}^\dagger)\sigma_y^T$, which gives rise to coherent energy exchange at the resonance between the charge qubit and the phase qubit (or the oscillator). The effects of this first term on the quantum dynamics of the circuit are similar to those produced by the capacitive coupling

term in $\hat{\sigma}_x^S\hat{\sigma}_x^T$ or $(\hat{a}-\hat{a}^\dagger)\sigma_x^T$. The second term $\hat{\sigma}_y^S\hat{\sigma}_z^T$ or $(\hat{a}-\hat{a}^\dagger)\sigma_z^T$ contains a transverse contribution for the SQUID and a longitudinal term which depends on the transistor qubit state. Its contribution will explain the quantum measurement of the charge qubit in the $\nu_S \ll \nu_T$ limit (see Sec. VI C). We notice finally that the two terms are strongly tunable with the bias parameter δ.

VI. ANALYSIS OF THE COUPLED CIRCUIT HAMILTONIAN

The full Hamiltonian of the coupled circuit is given by the sum of the Hamiltonians of the dc SQUID, the ACPT and the coupling. It reads $\widehat{H}=\widehat{H}_S+\widehat{H}_{\rm ACPT}+\widehat{H}_{\rm Coupl,Capa}+\widehat{H}_{\rm Coupl,Jos}$. In order to simplify this Hamiltonian, we consider hereafter the situation where the gate-charge is fixed to $n_g=0.5$. This charge value has been mainly used for the charge qubits experiments (see Refs. 15 and 35). Indeed, at $n_g=0.5$, the charge qubit is insensitive in first order to charge noise and, therefore, its coherence time is longer. We will first derive the expression of the full Hamiltonian when the two quantum systems are close to the resonance condition. We will consider the dc SQUID either as a phase qubit or as a harmonic oscillator. Finally, we will discuss the quantum measurement scenario of the transistor states. Its principle derives from the coupling to the SQUID, enabling to use it as a detector of the charge qubit state.

A. A charge qubit coupled to a phase qubit

We first consider the dc SQUID as a phase qubit such that the full Hamiltonian governs the quantum dynamics of two-coupled qubits. Using the expressions of the Josephson and capacitive coupling in that limit, we find

$$\widehat{H}=\frac{h\nu_S}{2}\hat{\sigma}_z^S+\frac{h\nu_T}{2}\hat{\sigma}_z^T-E_{c,c}\hat{\sigma}_x^S\hat{\sigma}_x^T +E_{c,j}\cos(\delta/2-\chi)\hat{\sigma}_y^S\hat{\sigma}_y^T-E_{c,j}\sin(\delta/2-\chi)\hat{\sigma}_y^S\hat{\sigma}_z^T. \tag{32}$$

Let us introduce the raising operators $\hat{\sigma}_+^T$ and $\hat{\sigma}_+^S$ and the lowering operators $\hat{\sigma}_-^T$ and $\hat{\sigma}_-^S$. These operators are defined by $\hat{\sigma}_\pm^T\equiv(\hat{\sigma}_x^T\pm i\hat{\sigma}_y^T)/2$ and $\hat{\sigma}_\pm^S\equiv(\hat{\sigma}_x^S\pm i\hat{\sigma}_y^S)/2$. The terms $\hat{\sigma}_x^S\hat{\sigma}_x^T$ and $\hat{\sigma}_y^S\hat{\sigma}_y^T$ can be written using the four products $\hat{\sigma}_+^S\hat{\sigma}_-^T$, $\hat{\sigma}_-^S\hat{\sigma}_+^T$, $\hat{\sigma}_+^S\hat{\sigma}_+^T$, and $\hat{\sigma}_-^S\hat{\sigma}_-^T$, whereas the term $\hat{\sigma}_y^S\hat{\sigma}_z^T$ is a function of the operators $\hat{\sigma}_+^S\hat{\sigma}_z^T$ and $\hat{\sigma}_-^S\hat{\sigma}_z^T$.

The product $\hat{\sigma}_+^S\hat{\sigma}_-^T$ corresponds to an excitation of the phase qubit and deexcitation of the charge qubit. This coupling term mediates the transition between the states $|0,+\rangle$ and $|1,-\rangle$. This transition is only relevant close to resonance, where it contributes to the low-frequency dynamics of the coupled system. Far away from resonance, this term gives rise to high-frequency dynamics (frequencies of the order of ν_S and ν_T) which is averaged away on the typical time scales of the experiment.[17] The rotating-wave approximation consists in neglecting these nonresonant terms, called also inelastic terms. The previous reasoning applied to the term $\hat{\sigma}_-^S\hat{\sigma}_+^T$ leads to the same result. The products $\hat{\sigma}_+^S\hat{\sigma}_+^T$ and $\hat{\sigma}_-^S\hat{\sigma}_-^T$ couple the states $|0,-\rangle$ and $|1,+\rangle$. The transition between these two states leads to high-frequency dynamics and are neglected hereafter. For the same reason, the coupling term $\hat{\sigma}_y^S\hat{\sigma}_z^T$ will be ignored. Finally, close to the resonance, the full Hamiltonian simplifies to

$$\widehat{H}=\frac{h\nu_S}{2}\hat{\sigma}_z^S+\frac{h\nu_T}{2}\hat{\sigma}_z^T-\frac{g}{2}(\hat{\sigma}_+^S\hat{\sigma}_-^T+\hat{\sigma}_-^S\hat{\sigma}_+^T), \tag{33}$$

where the coupling strength g is given by $g=2E_{c,c}-2E_{c,j}\cos(\delta/2-\chi)$. We assume hereafter that the gate capacitance $C_g \ll C_2^T$ and $C_1^T \ll C_0$, which is true for the measured circuits in Refs. 15 and 17. In these limits, we have $C_{n\|}\approx 2C_0(C_2^T+C_1^T)/(\alpha_\| C_2^T)$. The coupling energy can then be written as a function of the capacitance (λ) and Josephson (μ) asymmetries of the ACPT as

$$g=\frac{\alpha_\|}{2}\sqrt{\frac{E_C^\|}{h\nu_p}}\left[(1+\lambda)h\nu_p-(1+\mu)E_J^T\cos(\delta/2-\chi)\right]. \tag{34}$$

Further simplification of the coupling energy can be obtained using the fact that the charge qubit is described with two charge states, and that the SQUID has a zero anharmonicity. Then, the transistor frequency is related to δ by $\nu_T=(E_J^T/h)[\cos^2(\delta/2)+\mu^2\sin^2(\delta/2)]^{1/2}$ (see Sec. IV B) and we have $\nu_p=\nu_S$. By using these relations, the coupling g (34) can be rewritten as

$$g=\frac{\alpha_\|}{2}\sqrt{\frac{E_C^\|}{\nu_S}}\left[(1+\lambda)\nu_S-(1+\mu)\nu_T\left(\cos^2(\chi)+\frac{\sin^2(\chi)}{\mu}\right)\right]. \tag{35}$$

Note that coupling g depends strongly on the bias parameters, via the phase δ and the frequency ν_S. Therefore, the proposed circuit presents an intrinsic tunable coupling between a charge and a phase qubit, which we will analyze in more detail in Sec. VII. This transverse coupling enables to realize two-qubit gates operation as, for example, the $\sqrt{\rm iSWAP}$ operation.[36] Indeed gate operations can take advantage of the tunability of the energy and the coupling strength of the qubits. The single-qubit operation should be realized in the weak-coupling regime at the optimal point of the ACPT ($\delta=0, n_g=1/2$) and along the optimal line of the phase qubit ($I_b=0$). The two-qubit gate operations should be realized at the working point $n_g=1/2$ and in the vicinity of $\delta=\pi$. At this working point, the entangled system is insensitive to charge noise. In addition, the coupling strength is maximal enabling fast qubit operation.

B. A charge qubit coupled to a tunable harmonic oscillator

The Hamiltonian (33), which governs the dynamics of two coupled qubits, is valid if the second and highest levels of the dc SQUID do not participate in the quantum dynamics of the circuit. This is the case when the anharmonicity of the SQUID is sufficiently strong. In the limit of zero anharmonicity, the Hamiltonian of the coupled circuit is described by the Jaynes-Cummings Hamiltonian[37]

$$\widehat{H}=h\nu_p\left(\hat{a}\hat{a}^\dagger+\frac{1}{2}\right)+\frac{h\nu_T}{2}\hat{\sigma}_z^T-\frac{g}{2}(\hat{a}^\dagger\hat{\sigma}_-^T+\hat{a}\hat{\sigma}_+^T). \tag{36}$$

This Hamiltonian (36) is very similar to the one obtained by coupling a charge[38] or a transmon[39] or phase qubit[40] to a coplanar waveguide cavity. In our circuit the resonator is realized by a micro dc SQUID. It can be viewed as a "microresonator" that is more convenient for integration than the usual coplanar resonators since its size ranges in a micrometer scale three orders of magnitude smaller. Moreover, its resonance frequency is strongly tunable. However, up to now it suffers from a much shorter coherence time.

C. Quantum measurements of the charge qubit by the dc SQUID

Our theoretical analysis introduces two different kinds of coupling which can be used to perform quantum measurements of the charge qubit by the dc SQUID. Here we will apply this analysis to the quantronium readout[15] and the adiabatic quantum transfer method used in Ref. 17.

1. Quantronium readout

This readout is obtained in the limit where $\nu_T \gg \nu_S$. As we will see, even if the qubits are far from resonance, the coupling still affects the dynamics of the circuit. Indeed, since the dynamics of the ACPT is much faster than the dc SQUID dynamics, the dc SQUID is only sensitive to the average value of the ACPT operators. After some straightforward algebra, the effective Hamiltonian of the dc SQUID takes the following form:

$$\hat{H}^{|\pm\rangle}_{S,\mathrm{eff}} = \widehat{H}_S - \frac{C_T}{C_{n\|}}\frac{\partial E_{|\pm\rangle}}{\partial n_g}\widetilde{P}_\| + \alpha_\|\frac{\partial E_{|\pm\rangle}}{\partial \delta}\widetilde{X}_\|, \tag{37}$$

with $E_{|+\rangle}$ and $E_{|-\rangle}$ the eigenenergies of the ACPT associated with the states $|+\rangle$ and $|-\rangle$. For $n_g = 0$ or $n_g = 1/2$, we have $\partial E_{|\pm\rangle}/\partial n_g = 0$ and the SQUID Hamiltonian simplifies to

$$\hat{H}^{|\pm\rangle}_{S,\mathrm{eff}} = \widehat{H}_S - \phi_0 I^{|\pm\rangle}_{\mathrm{add}}\widetilde{X}_\|, \tag{38}$$

where $I^{|\pm\rangle}_{\mathrm{add}} \equiv -(\alpha_\|/\phi_0)\partial E_{|\pm\rangle}/\partial\delta$ adds to the bias current I_b and depends on the state of the ACPT $|-\rangle$ or $|+\rangle$. For $n_g = 1/2$, in the limit of two charge states only, the additional current reads

$$I^{|\pm\rangle}_{\mathrm{add}}(n_g = 1/2) = \pm\frac{E_J^T}{2\phi_0}(1+\mu)\sin(\delta/2 - \chi). \tag{39}$$

The currents $I^{|+\rangle}_{\mathrm{add}}(n_g = 1/2)$ and $I^{|-\rangle}_{\mathrm{add}}(n_g = 1/2)$ take opposite values and, therefore, can be used to determine the transistor state. Figure 13 shows the normalized current $I^{|-\rangle}_{\mathrm{add}}/(E_J^T/2\phi_0)$ for $n_g = 1/2$ as a function of the phase δ for an asymmetric ($\mu = 0.42$) and a symmetric ($\mu = 0$) transistor and a Cooper pair box ($\mu = 1$). For a symmetric transistor, the current has a strong discontinuity at $\delta = \pm\pi$ jumping between the two extreme values $-E_J^T/2\phi_0$ and $E_J^T/2\phi_0$. This discontinuity disappears for a finite Josephson asymmetry; its maximum value is lower. Naturally, for a Cooper pair box, the additional current is zero as one of the junctions is replaced by a pure capacitance.

As the switching probability of the dc SQUID depends strongly on the bias current[30] the additional current I_{add} can be used to detect the ACPT state. For instance, in the quantronium circuit,[15] the state of a symmetric Cooper pair transistor

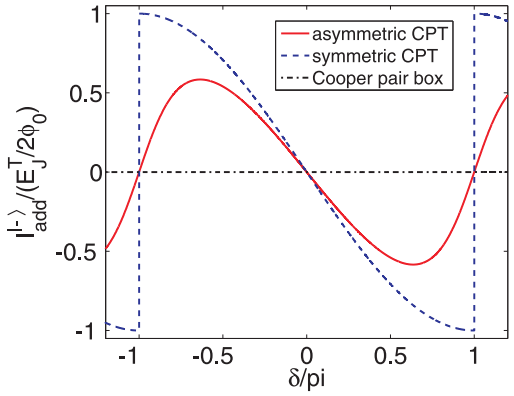

FIG. 13. (Color online) Effective current $I^{|-\rangle}_{\mathrm{add}}$ at $n_g = 1/2$ as a function of the phase δ for an asymmetric ($\mu = 0.42$) and symmetric ($\mu = 0$) transistors and a Cooper pair box ($\mu = 1$).

(CPT) is read out by measuring the switching probability of a Josephson junction placed in parallel with the CPT and which replaces the dc SQUID in the studied circuit. In that case, the charge qubit readout is explained by the $\widehat{X}^S_\|\hat{\sigma}^T_z$ term resulting from the Josephson coupling (28).

Expression (39) of the additional current has been established under the condition $\nu_T \gg \nu_S$. Is this expression still valid when $\nu_T \approx \nu_S$? In order to answer this question, we compare experimental data and theoretical predictions for the difference of the additional currents at $n_g = 1/2$ and $n_g = 0$ in the ground state of the ACPT. This difference noted $\Delta I^-_{\mathrm{add}} \equiv I^{|-\rangle}_{\mathrm{add}}(n_g = 1/2) - I^{|-\rangle}_{\mathrm{add}}(n_g = 0)$ is shown in Fig. 14 as a function of the flux Φ_S. The theoretical curve calculated without any free parameters agrees well with the experiment when $\nu_T/\nu_S \gg 1$, but differs from the experiment when $\nu_T \approx \nu_S$. The measured current amplitude drops when ν_T is close to ν_S, suggesting a drop in the contrast of the quantum measurement when $\nu_T \approx \nu_S$.

2. Adiabatic quantum transfer

In Fig. 15, the first energy levels of the charge and phase qubit in the coupled circuits are plotted. The quantum measurement of the charge qubit is performed by a nanosecond flux pulse which transfers the quantum state $|0,+\rangle$ prepared at the working point $(I_b^{\mathrm{wp}},\Phi_S^{\mathrm{wp}})$ to the measurement point $(I_b^{\mathrm{esc}},\Phi_S^{\mathrm{esc}})$. At that point the SQUID is very close to the critical line and the escape probability is finite. Spectroscopy measurements show clearly the readout of the charge qubit by this method even in the limit $\nu_T \approx \nu_S$. How can we explain this readout?

The coupling terms $\hat{\sigma}^S_+\hat{\sigma}^T_-$ and $\hat{\sigma}^S_-\hat{\sigma}^T_+$ produce an antilevel crossing, whose amplitude depends on the coupling strength g [see the inset of Fig. 15(c)]. During a nanosecond flux pulse, the coupled system remains in its original energy state; as a result, the quantum state $|0,+\rangle$ evolves adiabatically into the state $|1,-\rangle$. Due to a large value of the coupling strength close to the escape point, Landau-Zener transitions can be neglected. The final state, i.e., $|1,-\rangle$ or $|0,-\rangle$, is determined by the switching measurement.

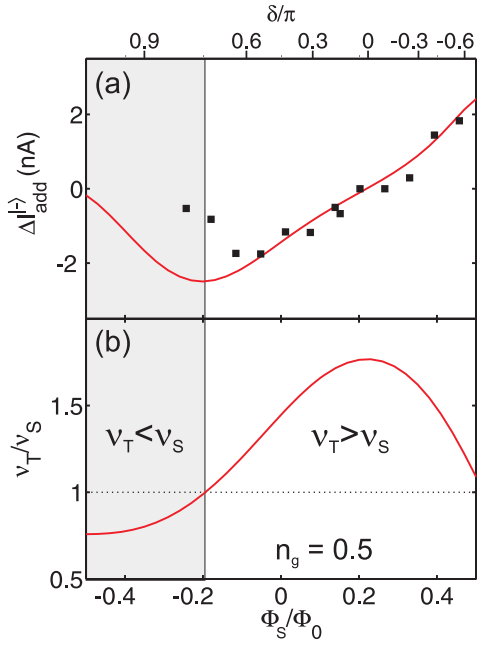

FIG. 14. (Color online) (a) Experimental (black squares) and theoretical (red line) current difference $\Delta I^{|-\rangle}_{\rm add} \equiv I^{|-\rangle}_{\rm add}(n_g = 1/2) - I^{|-\rangle}_{\rm add}(n_g = 0)$ as a function of the flux Φ_S (or the phase δ indicated in the upper scale). (b) Frequencies ratio ν_T/ν_S as a function of Φ_S.

VII. TUNABLE COUPLING

In this section, we calculate numerical values of the coupling strength g, using the circuit parameters of Ref. 17, and show that the coupling can be tuned over a wide range with the bias parameters.

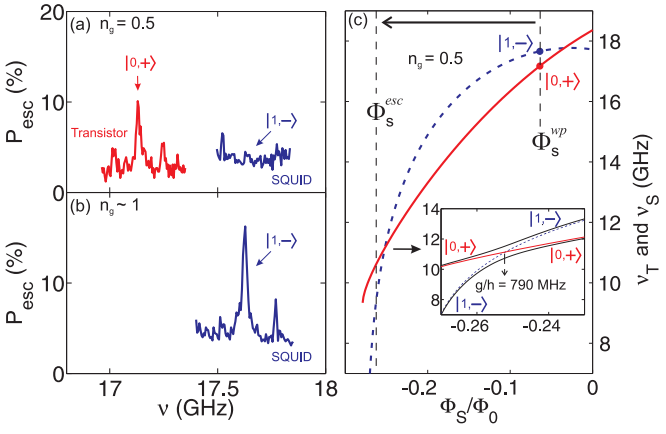

FIG. 15. (Color online) Spectroscopies of the phase (blue curve) and charge (red curve) qubit studied in Ref. 17 at (a) $n_g = 0.5$ and (b) $n_g \approx 1$ ($\nu_T \gg \nu_S$) for the working point ($I_b^{\rm wp} = 1957$ nA, $\Phi_S^{\rm wp} = -0.064\ \Phi_0$). These spectroscopies are measured with a nanosecond flux pulse which changes the flux in the SQUID loop from $\Phi_S^{\rm wp}$ to $\Phi_S^{\rm esc}$. (c) Evolution of the qubit frequencies ν_T and ν_S during this pulse. Blue and red points indicate the frequencies ν_S and ν_T at the working point of spectroscopy (a). The inset shows an antilevel crossing in the energy spectrum where an adiabatic transfer happens during the flux pulse, the state $|1,-\rangle$ ($|0,+\rangle$) being transferred to the state $|0,+\rangle$ ($|1,-\rangle$).

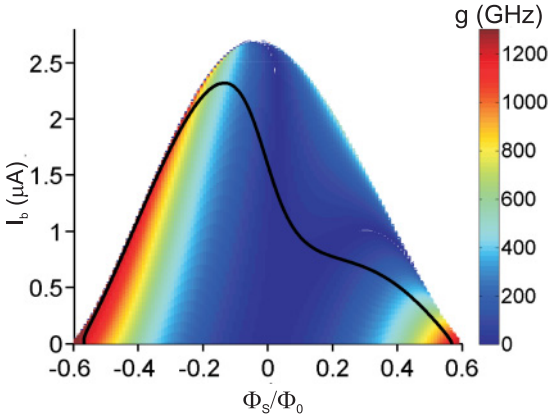

FIG. 16. (Color online) Color plot of the analytical coupling (35) as a function of the bias current I_b and the flux Φ_S, for the well family [0] of the dc SQUID. The solid line indicates where the two qubits are in resonance ($\nu_S = \nu_T$).

Figure 16 presents the dependence of the coupling g as a function of the bias current I_b and the flux Φ_S for the family [0] of the dc SQUID. We find that the coupling between the two qubits can be tuned from zero to more than 1.2 GHz. This on-off coupling is one of the needed requirements to realize ideally one- and two-qubit gates. In Ref. 17, the coupling g has been measured at resonance, where the coupling effect on the qubits is maximal. Far away from resonance, the eigenenergies of each individual qubit are shifted by the amount $g^2/4|\Delta|$, where $\Delta = h\nu_S - h\nu_T$ is the detuning. So, if the detuning is large the coupling can be neglected. The solid line of Fig. 16 shows where the qubits are in resonance and, consequently, where the coupling can be easily measured by spectroscopy.

Figure 17 shows the dependence of the coupling g as a function of the phase δ for three different charge qubits: an asymmetric transistor,[17] a symmetric transistor,[15] and a Cooper pair box.[35] The coupling has been calculated using expression (35) at the resonance $\nu_S = \nu_T$ with the parameters of Ref. 17 and only the ACPT asymmetries have been varied.

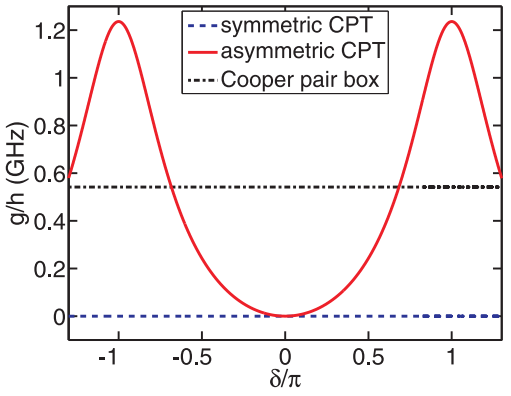

FIG. 17. (Color online) Coupling g derived from Eq. (35) as a function of δ when the two qubits are in resonance ($\nu_T = \nu_S$) for three different charge qubits: (red curve) an asymmetric transistor with $\lambda = \mu = -41.6\%$, (blue curve) a symmetric transistor $\lambda = \mu = 0$, and (black curve) a Cooper pair box with $\lambda = -41.6\%$ and $\mu = -1$. The calculations have been realized by using the parameters of Ref. 17 given in Appendix B.

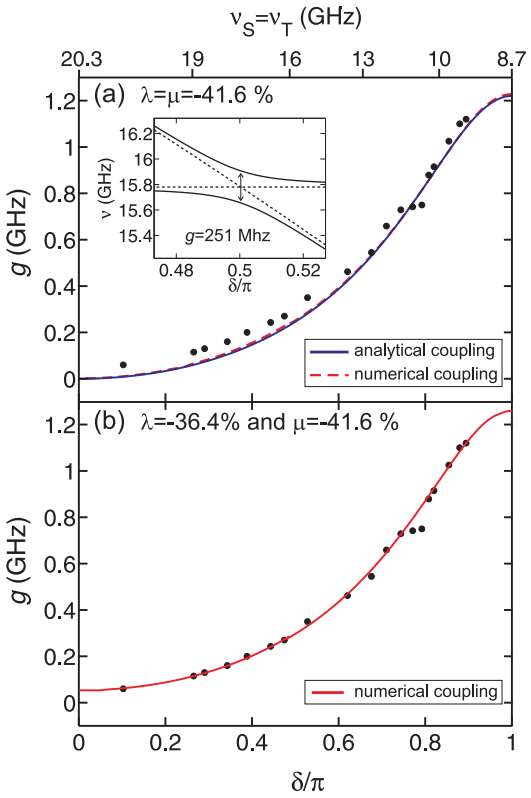

FIG. 18. (Color online) (a) Coupling g as a function of δ when the SQUID and the ACPT are in resonance ($\nu_T = \nu_S$). The black points are the experimental couplings measured in Ref. 17. The blue line is the theoretical coupling calculated from the analytical expression (35), using the circuit parameters of Ref. 17 and equal Josephson and capacitance asymmetries $\mu = \lambda = -46.6\%$. The red line is the numerical coupling for the same circuit parameters. It is calculated by diagonalizing the full Hamiltonian in the basis of eight charge states and the first nine harmonic dc SQUID states. The inset shows the numerical simulations of the eigenenergies of the circuit with (full curve) and without (dashed curve) coupling from which we extract the coupling $g/h = 251$ MHz at $\delta = 0.5\pi$. (b) Numerical coupling g as a function of δ when the SQUID and the ACPT are in resonance, calculated using the circuit parameters used in (a) but with a different capacitance asymmetry $\lambda = 0.87\mu = -36.4\%$.

For the asymmetric transistor with $\lambda = \mu = -41.6\%$, the coupling g (red curve) is maximum at $\delta = \pm\pi$ where it equals to 1217 MHz; it becomes zero at $\delta = 0$. In the case of the *symmetric* transistor with $\lambda = \mu = 0$, the coupling strength reads $g = \alpha_{\parallel}/2\sqrt{E_C^{\parallel}/\nu_S}(\nu_S - \nu_T)$. Consequently, at the resonance, the coupling between a *symmetric* transistor and a SQUID is zero. For a Cooper pair box with $E_{J2}^T = 0$ ($\mu = -1$ and $\lambda = -41.6\%$), the coupling reads $g = \frac{\alpha_{\parallel}}{2}\sqrt{E_C^{\parallel} h\nu_S}(1+\lambda)$. This corresponds to the result of Ref. 34. The calculated coupling g (black curve) does not depend on δ and remains equal to 514 MHz.

Figure 18(a) shows the dependence of the analytical and numerical couplings at the resonance as a function of the absolute value of the phase δ. The numerical simulations allow us to check the validity of the analytical coupling. These simulations have been realized by diagonalizing the full Hamiltonian in the basis of 20 charge states and the first nine excited states of the dc SQUID in the absence of anharmonicity. The dc SQUID and ACPT Hamiltonians, as well as the Josephson and capacitive coupling Hamiltonians, can all be expressed naturally in these bases. The numerical coupling is found by calculating the energy spectrum as a function of δ between $-\pi$ and π for a fixed frequency ν_S. The spectrum is first calculated without the coupling terms in order to find the two opposite values of $\delta = \pm\delta_r$, where the ACPT and the dc SQUID are in resonance ($\nu_S = \nu_T$), i.e., where the second and third energy bands intersect. In the presence of coupling, the degeneracy between the eigenstates is lifted and an antilevel crossing appears with an energy separation equal to the coupling g at $\delta = \pm\delta_r$. As an example, the inset of Fig. 18(a) shows the energy spectrum for $\delta_r = 0.5\pi$ with and without coupling from which we extract $g/h = 251$ MHz. The numerical and analytical simulations remarkably give quite close results, which confirms the validity of the analytical expression (35). The theoretical coupling is calculated here without any free parameters by assuming equal Josephson and capacitive asymmetries ($\lambda = \mu = -41.6\%$). Finally, we note the good agreement with the experimental coupling measured in Ref. 17 and shown in black points in Fig. 18. By adjusting the capacitive asymmetry to $\lambda = -36.4\%$ the numerical coupling is in perfect agreement with the experiment as shown in Fig. 18(b).

VIII. CONCLUSION

In conclusion, we have analyzed in detail the Hamiltonian of a superconducting circuit based on a dc SQUID in parallel to an asymmetric Cooper pair transistor (ACPT). The Lagrangian of the circuit was first established from the current conservation equations expressed at each node of the circuit. The Hamiltonian, deduced from the Lagrangian, is decomposed in three distinct terms, namely, the dc SQUID, the ACPT, and the coupling Hamiltonians. We first studied the individual Hamiltonians of the dc SQUID and the ACPT. Depending on its anharmonicity, the dc SQUID can be seen either as a harmonic oscillator or as a phase qubit, whereas the ACPT behaves as a charge qubit. In addition to the optimal bias points ($\delta = 0, n_g = 1/2$), which was successfully demonstrated in a symmetric Cooper pair transistor, the ACPT presents a second optimal point ($\delta = \pi, n_g = 1/2$). At these points, the charge qubit is insensitive in first order to the charge, flux, and current noise, and therefore shows a larger coherence time. We found that the coupling Hamiltonian between the dc SQUID and the ACPT is made of two different terms corresponding to the Josephson and the capacitive couplings, which mix phases and charges of both subcircuits, respectively.

The Hamiltonian of the full circuit was discussed through two different limits of the dc SQUID. When it behaves as a harmonic oscillator, the circuit is described by the well-known Jaynes-Cummings Hamiltonian. The microscopic circuit is then similar to a two-level atom coupled to a single-mode optical cavity. Compared to the latter, it offers a better tunability, a faster control and readout of the quantum system, and a good scalability for complex architecture implementation. For example, a circuit of several ACPT qubit in parallel could be considered whose quantum information will be mediated by

the dc SQUID.[41] When the anharmonicity of the dc SQUID is strong, it behaves as a phase qubit. The full circuit is then described as the coupling of two different class of qubits, i.e., a phase and a charge qubit. The coupling Hamiltonian contains terms in $\hat{\sigma}_y^T\hat{\sigma}_y^S$ and $\hat{\sigma}_x^T\hat{\sigma}_x^S$ which are prominent when the two qubits are in resonance. These terms allow two-qubit gate operations as the $\sqrt{\text{iSWAP}}$ gate. In addition, they enable to read out the quantum state of the ACPT by a nanosecond flux pulse as observed in Ref. 17. Indeed, such a pulse produces an adiabatic quantum transfer of the state $|0,+\rangle$ into the state $|1,-\rangle$, i.e., the energy quantum stored in the ACPT is transferred into the dc SQUID in order to be detected. A nonresonant term in $(\hat{a}-\hat{a}^\dagger)\hat{\sigma}_z^T$ or in $\hat{\sigma}_y^S\hat{\sigma}_z^T$ is present in the Josephson coupling. Although its effect on the energy spectrum of the circuit is weak, the latter term explains the charge qubit readout in the limit $\nu_T \gg \nu_S$ by means of an effective additional current in the dc SQUID. That readout method is employed in the quantronium circuit.[15]

In both limits of the dc SQUID, we demonstrated that the coupling can be strongly tuned, mainly with the Josephson coupling term, which has a strong phase δ dependence. It can be used to accomplish two-qubit gate operations, and can also be turned off in order to perform one-qubit gate operations without disturbing the unaddressed qubit.

ACKNOWLEDGMENTS

We thank J. Claudon, E. Hoskinson, L. Lévy, and D. Estève for fruitful discussions. This work was supported by the EuroSQIP, MIDAS, and SOLID European projects, by the French ANR'QuantJO', and by Institut Universitaire de France.

APPENDIX A: CURRENT CONSERVATION LAWS

The current conservation law, applied to each node of the circuit [see Fig. 1(b)], yields six equations for the active phases φ_1, φ_2, ψ, θ, and ξ. These equations are identical to the Euler-Lagrange equations derived from the circuit Lagrangian, (2)–(4) and read, respectively,

$$\phi_0\frac{\xi-\varphi_1}{L_1} - C_0\phi_0\ddot{\varphi}_1 - I_0\sin(\varphi_1) = 0, \tag{A1}$$

$$\phi_0\frac{\gamma-\varphi_2}{L_2} - C_0\phi_0\ddot{\varphi}_2 - I_0\sin\varphi_2 = 0, \tag{A2}$$

$$I_2^T\sin(\xi-\psi-\phi_T) + C_2^T\phi_0(\ddot{\xi}-\ddot{\psi}) - C_g\phi_0(\ddot{\psi}-\ddot{\theta}) - C_1^T\phi_0\ddot{\psi} - I_1^T\sin(\psi) = 0, \tag{A3}$$

$$C_g\ddot{\psi} - (C_P+C_g)\ddot{\theta} = 0, \tag{A4}$$

$$\phi_0\frac{\gamma-\xi-\phi_S}{L_3} - \phi_0\frac{\xi-\varphi_1}{L_1} - C_2^T\phi_0(\ddot{\xi}-\ddot{\psi}) - I_2^T\sin(\xi-\psi-\phi_T) = 0. \tag{A5}$$

In Sec. II C, we show that this system of six equations can be reduced to four equations by ignoring the high-frequency quantum dynamics of the phases γ and ξ.

TABLE IV. Electric parameters of the coupled circuit studied by Fay *et al.* (Ref. 17).

	Label	Value
Parameters of the dc SQUID		
Critical current per Josephson junction (JJ)	I_0	1.356 μA
Capacitance per JJ	C_0	227 fF
Loop inductance	L_s	190 pH
Inductance asymmetry	η	0.28
Bidimensionality parameter	b	1.28
Parameters of the ACPT		
Critical current of the first JJ	I_1^T	30.1 nA
Critical current of the second JJ	I_2^T	12.4 nA
Capacitance of the first JJ	C_1^T	2.0 fF
Capacitance of the second JJ	C_2^T	0.9 fF
Critical current asymmetry	μ	−41.6%
Capacitance asymmetry	λ	−37.7%
Gate capacitance	C_g	29 aF

APPENDIX B: PARAMETERS OF THE COUPLED CIRCUIT STUDIED IN Ref. 17

Throughout this article, we illustrate the theory with numerical values and plots calculated by using the parameters of the circuit studied in Ref. 17. These parameters are collected in Table IV.

APPENDIX C: CONJUGATE VARIABLES

The phases $(X_\parallel, Y_\perp, \psi, \theta)$ and their conjugate momenta $(-\hbar P_\parallel, -\hbar P_\perp, -\hbar n, -\hbar n_Q)$ are the appropriate variables of the circuit Hamiltonian (15). The momenta are related to the velocities $(\dot{X}_\parallel, \dot{Y}_\perp, \dot{\psi}, \dot{\theta})$ involved in the kinetic part of the Lagrangian (13) by the following expressions:[25]

$$-\hbar P_\parallel = \frac{\partial\mathcal{L}}{\partial\dot{X}_\parallel} = \phi_0^2\left\{\left(2C_0+\alpha_\parallel^2C_2^T\right)\dot{X}_\parallel - \alpha_\parallel C_2^T(\alpha_\perp\dot{Y}_\perp+\dot{\psi})\right\}, \tag{C1}$$

$$-\hbar P_\perp = \frac{\partial\mathcal{L}}{\partial\dot{Y}_\perp} = \phi_0^2\left\{\left(2C_0+\alpha_\perp^2C_2^T\right)\dot{Y}_\perp - \alpha_\perp C_2^T(\alpha_\parallel\dot{X}_\parallel-\dot{\psi})\right\}, \tag{C2}$$

$$-\hbar n = \frac{\partial\mathcal{L}}{\partial\dot{\psi}} = \phi_0^2\left\{C_\Sigma\dot{\psi} - C_2^T(\alpha_\parallel\dot{X}_\parallel - \alpha_\perp\dot{Y}_\perp) - C_g\dot{\theta}\right\}, \tag{C3}$$

$$-\hbar n_Q = \frac{\partial\mathcal{L}}{\partial\dot{\theta}} = \phi_0^2\left\{(C_P+C_g)\dot{\theta} - C_g\dot{\psi}\right\}. \tag{C4}$$

APPENDIX D: PAULI MATRIXES

The Pauli matrices related to the dc SQUID are defined in the eigenbasis of the phase qubit $\{|1\rangle,|0\rangle\}$ as

$$\sigma_z^S = \begin{pmatrix}1 & 0\\ 0 & -1\end{pmatrix}, \quad \sigma_x^S = \begin{pmatrix}0 & 1\\ 1 & 0\end{pmatrix}, \quad \sigma_y^S = \begin{pmatrix}0 & -i\\ i & 0\end{pmatrix}. \tag{D1}$$

Similarly the Pauli matrices related to the ACPT $(\sigma_z^T, \sigma_x^T, \sigma_y^T)$ are defined in the eigenbasis of the charge qubit $\{|+\rangle,|-\rangle\}$.

*Present address: Low Temperature Laboratory, Aalto University, P.O. Box 15100, FI-00076 AALTO, Finland.

[1]J. M. Raimond, M. Brune, and S. Haroche, Rev. Mod. Phys. **73**, 565 (2001).

[2]D. Leibfried, R. Blatt, C. Monroe, and D. Wineland, Rev. Mod. Phys. **75**, 565 (2003).

[3]C. Tannoudji-Cohen, J. Dupont-Roc, and G. Grynberg, *Photons and Atoms: Introduction to Quantum Electrodynamics* (Wiley Interscience, New York, 1997).

[4]A. Steane, Rept. Prog. Phys. **61**, 117 (1998).

[5]M. Hofheinz, H. Wang, M. Ansmann, R. C. Bialczak, E. Lucero, M. Neeley, A. D. OConnell, D. Sank, J. Wenner, J. M. Martinis, and A. N. Cleland, Nature (London) **459**, 546 (2009).

[6]L. DiCarlo, J. M. Chow, J. M. Gambetta, Lev S. Bishop, B. R. Johnson, D. I. Schuster, J. Majer, A. Blais, L. Frunzio, S. M. Girvin, and R. J. Schoelkopf, Nature (London) **460**, 240 (2009).

[7]A. Palacios-Laloy, F. Mallet, F. Nguyen, P. Bertet, D. Vion, D. Esteve, and A. N. Korotkov, Nat. Phys. **6**, 442 (2010).

[8]O. Astafiev, A. M. Zagoskin, A. A. Abdumalikov Jr., Yu. A. Pashkin, T. Yamamoto, K. Inomata, Y. Nakamura, and J. S. Tsai, Science **327**, 840 (2010).

[9]J. H. Plantenberg, P. C. de Groot, C. J. P. M. Harmans, and J. E. Mooij, Nature (London) **447**, 836 (2007).

[10]C. M. Wilson, T. Duty, F. Persson, M. Sandberg, G. Johansson, and P. Delsing, Phys. Rev. Lett. **98**, 257003 (2007).

[11]H. Nakano, S. Saito, and K. Semba, and H. Takayanagi, Phys. Rev. Lett. **102**, 257003 (2009).

[12]T. A. Palomaki, S. K. Dutta, R. M. Lewis, A. J. Przybysz, Hanhee Paik, B. K. Cooper, H. Kwon, J. R. Anderson, C. J. Lobb, F. C. Wellstood, and E. Tiesinga, Phys. Rev. B **81**, 144503 (2010).

[13]E. Hoskinson, F. Lecocq, N. Didier, A. Fay, F. W. J. Hekking, W. Guichard, O. Buisson, R. Dolata, B. Mackrodt, and A. B. Zorin, Phys. Rev. Lett. **102**, 097004 (2009).

[14]Y. Makhlin, G. Schön, and A. Shnirman, Rev. Mod. Phys. **73**, 357 (2001).

[15]D. Vion, A. Aassime, A. Cottet, P. Joyez, H. Pothier, C. Urbina, D. Estève, and M. H. Devoret, Science **296**, 886 (2002).

[16]N. Boulant, G. Ithier, P. Meeson, F. Nguyen, D. Vion, D. Estève, I. Siddiqi, R. Vijay, C. Rigetti, F. Pierre, and M. Devoret, Phys. Rev. B **76**, 014525 (2007).

[17]A. Fay, E. Hoskinson, F. Lecocq, L. P. Lévy, F. W. J. Hekking, W. Guichard, and O. Buisson, Phys. Rev. Lett. **100**, 187003 (2008).

[18]A. Wallraff, D. I. Schuster, A. Blais, L. Frunzio, R.-S. Huang, J. Majer, S. Kumar, S. M. Girvin, and R. J. Schoelkopf, Nature (London) **431**, 162 (2004).

[19]B. Yurke and J. S. Denker, Phys. Rev. A **29**, 1419 (1984).

[20]M. H. Devoret, *Quantum Fluctuations in Electrical Circuits*, Les Houches, Session LXIII (Elsevier, Amsterdam, 1995), Chap. 10.

[21]G. Burkard, R. H. Koch, and D. P. DiVincenzo, Phys. Rev. B **69**, 064503 (2004).

[22]T. P. Orlando, J. E. Mooij, Lin Tian, Caspar H. van der Wal, L. S. Levitov, Seth Lloyd and J. J. Mazo, Phys. Rev. B **60**, 15398 (1999).

[23]M. Tinkham, *Introduction to Superconductivity* (McGraw-Hill, New York, 1996), 2nd ed., Vol. 1.

[24]B. D. Josephson, Phys. Lett. **1**, 251 (1962).

[25]L. D. Landau and E. M. Lifshitz, *Mechanics*, 3rd ed. (Pergamon, Oxford, 1976).

[26]In Ref. 17, the inductance asymmetry η comes from the difference between the length of the two dc SQUID arms.

[27]J. Claudon, F. Balestro, F. W. J. Hekking, and O. Buisson, Phys. Rev. Lett. **93**, 187003 (2004).

[28]V. Lefevre-Seguin, E. Turlot, C. Urbina, D. Estève, and M. H. Devoret, Phys. Rev. B **46**, 5507 (1992).

[29]A. Fay, Ph.D. thesis, Université Joseph Fourier (Grenoble I), 2008; [http://tel.archives-ouvertes.fr/tel-00310131/fr/].

[30]J. Claudon, A. Fay, E. Hoskinson, and O. Buisson, Phys. Rev. B **76**, 024508 (2007).

[31]F. Balestro, J. Claudon, J. P. Pekola, and O. Buisson, Phys. Rev. Lett. **91**, 158301 (2003).

[32]D. A. Averin, K. K. Likharev, in *Quantum Effects in Small Disordered Systems*, edited by B. L. Al'tshuler, P. A. Lee, and R. A. Webb (Elsevier, Amsterdam, 1991).

[33]O. Buisson and F. W. J. Hekking, in *Macroscopic Quantum Coherence and Computing*, edited by D. Averin, B. Ruggiero, and P. Silvestrini (Kluwer Academic, New York, 2001), p. 137.

[34]O. Buisson and F. Balestro and J. P. Pekola and F. W. J. Hekking, Phys. Rev. Lett. **90**, 238304 (2003).

[35]Y. Nakamura, Yu. A. Pashkin, and J. S. Tsai, Nature (London) **398**, 786 (1999).

[36]Matthias Steffen, M. Ansmann, Radoslaw C. Bialczak, N. Katz, Erik Lucero, R. McDermott, Matthew Neeley, E. M. Weig, A. N. Cleland, and John M. Martinis, Science **313**, 1423 (2006).

[37]E. T. Jaynes and F. W. Cummings, Proc. IEEE **51**, 89 (1963).

[38]Alexandre Blais, Ren-Shou Huang, Andreas Wallraff, S. M. Girvin, and R. J. Schoelkopf, Phys. Rev. A **69**, 062320 (2004).

[39]Jens Koch, Terri M. Yu, Jay Gambetta, A. A. Houck, D. I. Schuster, J. Majer, Alexandre Blais, M. H. Devoret, S. M. Girvin, and R. J. Schoelkopf, Phys. Rev. A **76**, 042319 (2007).

[40]M. Sillanpää, J. I. Park, and R. W. Simmonds, Nature (London) **449**, 438 (2007).

[41]F. Plastina and G. Falci, Phys. Rev. B **67**, 224514 (2003).